



Univerza v Mariboru

Fakulteta za energetiko

Journal of ENERGY TECHNOLOGY



Volume 3 / Issue 4

NOVEMBER 2010

www.fe.uni-mb.si/si/jet.html

JOURNAL OF ENERGY TECHNOLOGY



VOLUME 3 / Issue 4

Revija Journal of Energy Technology (JET) je indeksirana v naslednjih bazah: INSPEC[®], Cambridge Scientific Abstracts: Abstracts in New Technologies and Engineering (CSA ANTE), ProQuest's Technology Research Database.

The Journal of Energy Technology (JET) is indexed and abstracted in the following databases: INSPEC[®], Cambridge Scientific Abstracts: Abstracts in New Technologies and Engineering (CSA ANTE), ProQuest's Technology Research Database.

JOURNAL OF ENERGY TECHNOLOGY

Ustanovitelj / FOUNDER

Fakulteta za energetiko, UNIVERZA V MARIBORU /
FACULTY OF ENERGY TECHNOLOGY, UNIVERSITY OF MARIBOR

Izdajatelj / PUBLISHER

Fakulteta za energetiko, UNIVERZA V MARIBORU /
FACULTY OF ENERGY TECHNOLOGY, UNIVERSITY OF MARIBOR

Izdajateljski svet / PUBLISHING COUNCIL

Zasl. Prof. dr. Dali ĐONLAGIĆ,

Univerza v Mariboru, Slovenija, **predsednik** / University of Maribor, Slovenia, **President**

Prof.dr. Bruno CVIKL,

Univerza v Mariboru, Slovenija / University of Maribor, Slovenia

Prof.ddr. Denis ĐONLAGIĆ,

Univerza v Mariboru, Slovenija / University of Maribor, Slovenia

Prof. dr. Danilo FERETIĆ,

Sveučilište u Zagrebu, Hrvatska / University in Zagreb, Croatia

Prof.dr. Roman KLASINC,

Technische Universität Graz, Avstrija / Graz University Of Technology, Austria

Prof.dr. Alfred LEIPERTZ,

Universität Erlangen, Nemčija / University of Erlangen, Germany

Prof. dr. Milan MARČIČ,

Univerza v Mariboru, Slovenija / University of Maribor, Slovenia

Prof.dr. Branimir MATIJAŠEVIČ,

Sveučilište u Zagrebu, Hrvatska / University in Zagreb, Croatia

Prof.dr. Borut MAVKO,

Inštitut Jožef Stefan, Slovenija / Jozef Stefan Institute, Slovenia

Prof.dr. Greg NATERER,

University of Ontario, Kanada / University of Ontario, Canada

Prof.dr. Enrico NOBILE,

Università degli Studi di Trieste, Italia / University of Trieste, Italy

Prof.dr. Iztok POTRČ,

Univerza v Mariboru, Slovenija / University of Maribor, Slovenia

Prof.dr. Andrej PREDIN,

Univerza v Mariboru, Slovenija / University of Maribor, Slovenia

Prof. dr. Jože VORŠIČ,

Univerza v Mariboru, Slovenija / University of Maribor, Slovenia

Prof.dr. Koichi WATANABE,

KEIO University, Japonska / KEIO University, Japan

Odgovorni urednik / EDITOR-IN-CHIEF

Andrej PREDIN

Uredniki / CO-EDITORS

Jurij AVSEC
Gorazd HREN
Milan MARČIČ
Iztok POTRČ
Janez USENIK
Jože VORŠIČ
Jože PIHLER

Uredniški odbor / EDITORIAL BOARD

Prof. dr. Jurij AVSEC,
Univerza v Mariboru, Slovenija / University of Maribor, Slovenia

Prof. ddr. Denis ĐONLAGIĆ,
Univerza v Mariboru, Slovenija / University of Maribor, Slovenia

Prof. dr. Roman KLASINC,
Technische Universität Graz, Avstrija / Graz University Of Technology, Austria

Dr. Ivan Aleksander KODELI
Institut Jožef Stefan, Slovenija / Jožef Stefan Institute, Slovenia

Prof. dr. Jurij KROPE,
Univerza v Mariboru, Slovenija / University of Maribor, Slovenia

Prof. dr. Alfred LEIPERTZ,
Universität Erlangen, Nemčija / University of Erlangen, Germany

Prof. dr. Branimir MATIJAŠEVIČ,
Sveučilište u Zagrebu, Hrvaška / University of Zagreb, Croatia

Prof. dr. Matej MENCINGER,
Univerza v Mariboru, Slovenija / University of Maribor, Slovenia

Prof. dr. Greg NATERER,
University of Ontario, Kanada / University of Ontario, Canada

Prof. dr. Enrico NOBILE,
Università degli Studi di Trieste, Italija / University of Trieste, Italy

Prof. dr. Iztok POTRČ,
Univerza v Mariboru, Slovenija / University of Maribor, Slovenia

Prof. dr. Andrej PREDIN,
Univerza v Mariboru, Slovenija / University of Maribor, Slovenia

Prof. dr. Aleksandar SALJNIKOV,
Univerza Beograd, Srbija / University of Beograd, Serbia

Prof. dr. Brane ŠIROK,
Univerza v Ljubljani, Slovenija / University of Ljubljana, Slovenia

Doc. dr. Andrej TRKOV,
Institut Jožef Stefan, Slovenija / Jožef Stefan Institute, Slovenia

Prof. ddr. Janez USENIK,
Univerza v Mariboru, Slovenija / University of Maribor, Slovenia

Prof. dr. Jože VORŠIČ,
Univerza v Mariboru, Slovenija / University of Maribor, Slovenia

Doc. Dr. Peter VIRTič,
Univerza v Mariboru, Slovenija / University of Maribor, Slovenia

Prof. dr. Koichi WATANABE,
KEIO University, Japonska / KEIO University, Japan

Doc. dr. Tomaž ŽAGAR,

Univerza v Mariboru, Slovenija / University of Maribor, Slovenia

Doc. dr. Franc ŽERDIN,

Univerza v Mariboru, Slovenija / University of Maribor, Slovenia

Tehniška podpora / TECHNICAL SUPPORT

Tamara BREČKO,

Sonja NOVAK,

Janko OMERZU;

Izhajanje revije / PUBLISHING

Revija izhaja štirikrat letno v nakladi 300 izvodov. Članki so dostopni na spletni strani revije - www.fe.uni-mb.si/si/jet.html .

The journal is published four times a year. Articles are available at the journal's home page - www.fe.uni-mb.si/si/jet.html .

Lektoriranje / LANGUAGE EDITING

Terry T. JACKSON

Produkcija / PRODUCTION

Vizualne komunikacije comTEC d.o.o.

Oblikovanje revije in znaka revije / JOURNAL AND LOGO DESIGN

Andrej PREDIN

Revija JET je sofinancirana s strani Javne agencije za knjigo Republike Slovenije.

The Journal of Energy Technology is co-financed by the Slovenian Book Agency.

Svetovni kongres energetike v Montrealu 2010

Septembra je potekal svetovni kongres energetike v Montrealu v Kanadi. Delegati so bili nekako mnenja, da bo na energetskega področju kratkoročno še naprej potekalo v znamenju težke nafte in premoga, saj večina držav tretjega dela sveta nima sredstev in ne možnosti doseganja novih, naprednejših energetskih tehnologij. V prvi vrsti so izpostavili, da je preskrba in možnost svetovnih potreb po energiji tista, ki lahko zagotovi trajno ekonomsko rast držav. Seveda se ob tem ne sme izpuščati okolja in okoljske problematike. To je torej izziv, ki združuje razvoj konvencionalnih energijskih virov in razvoj novih alternativnih energetskih tehnologij. Zato bomo morali agresivneje stopati po dveh vzporednih poteh. Kot prvo bomo morali biti kreativnejši pri iskanju in razvijanju tehnologij, ki temeljijo na konvencionalnih energijskih virih, pa najsi bodo to nafta, plin ali nuklearna energija, tako, da bodo ekonomsko, sociološko in okoljsko sprejemljive. Drugič, morali bomo uporabljati te konvencionalne energetske vire tako, da bomo pospešili raziskave in razvoj alternativne energetike, oz. razvoju novih energetskih tehnologij, ki bazirajo na alternativnih energetskih virih.

Mnogo je bilo diskusij okrog znižanja izpustov ogljikovega dioksida (CO₂), vendar je bilo le malo povedanega o zagotavljanju energije za vse in znižanju energetske potratnosti.

Alternativni energijski viri, kot so solarna tehnika, veter, geotermalni viri in bio-goriva, morajo predstavljati večji del v energetskega »miks«. Vendar je razvoj teh alternativ razmeroma počasen proces, kar pa nakazuje, da bo raba ogljikovodikov v energetiki še v naslednjem desetletju dominantna. Raba jedrske energije ni edina rešitev znižanja izpustov ogljikovega dioksida, omogoča pa oz. je uspešna alternativa drugim konvencionalnim energetskim virom, predvsem ogljikovodičnim tehnologijam. Zato mora jedrska energetika biti prepoznana kot ključna komponenta novega energetskega »miksa«.

Učinkovite in trajnostne energetske rešitve so potrebne za ohranjanje okolja, zato mora jedrska energetika biti sprejeta kot ključni dejavnik znotraj energetskega »miksa«, v naslednjih letih. V kolikor resnično želimo znižati emisije na energetskega področju, moramo razviti takšne tehnologije ki ne emitirajo v okolje, to pa pomeni razvoj obnovljivih in jedrskih energetskih tehnologij. Ti dve vrsti tehnologij se med seboj zelo dobro ujemata, saj je jedrski del stabilen in trajen vir, dočim so obnovljivi energetski viri razmeroma nestabilni. Res je, da je gradnja jedrskih postrojev draga, vendar pa se na dolgi rok zelo izplača, saj je proizvedena električna energija cenovno zelo konkurenčna. V primerjavi z ogljikovodičnimi tehnologijami je jedrsko gorivo cenovno zelo sprejemljivo in predvsem konstantno, dočim so cene ogljikovodičnih goriv nestabilne saj trg teh energentov zelo niha, oz. je odvisen od mnogih dejavnikov. Za gospodarsko ras je privlačna prav stabilna in nizka cena električne energije.

Glede izpostavljenih jedrskih odpadkov imamo že danes na voljo predelovalne tehnologije, samo aplicirati jih moramo čim prej. Danes znamo reciklirati 96% iztrošenega jedrskega goriva, tako, da ostaja problem samo 4% iztrošenega goriva. Zato potrebujemo javno sprejemljivost in v Sloveniji obstaja, saj smo se že odločili postaviti novo odlagališče jedrskih odpadkov v bližini obstoječe lokacije NEK v Vrbinu pri Krškem.

Menim in upam, da bo Slovenija našla pot na energetskega področju in se odločila za pravilno energetskega mešanico, predvsem z rabo trajnostnih energetskih virov kamor sodijo

jedrske in obnovljive energetske tehnologije. Na področju jedrske energetike imamo 40 let izkušenj, z zanesljivim in varnim obratovanjem obstoječe jedrske elektrarne Krško. Zato bi kazalo te izkušnje in znanja na področju jedrskih tehnologij ohraniti in uporabiti tudi v bodoče. Na področju rabe obnovljivih virov imamo prav tako zelo dobre izkušnje in znanje, kako graditi, voditi, upravljati in vzdrževati tehnologije, ki koristijo obnovljive energetske vire. Vključiti moramo še čim več alternativnih tehnologij (sonce, veter, geotermija) in tako uporabiti še ta razpoložljivi potencial. Seveda ob vsem naštetem ne smemo pozabiti na učinkovito energetske rabo, saj bomo tako najučinkoviteje prispevali k ohranitvi našega okolja in našega edinega planeta – Zemlje.

World Energy Congress in Montreal, 2010

The World Energy Congress was held in Montreal, Canada in September. Delegates were somehow considered to be “short on energy” continue to be affected by heavy oil and coal, while most of the developing world has no assets and no possibility of achieving a new, more advanced energy technologies. Ensuring energy availability in a world that needs to sustain economic growth, while respecting the environment is a challenge. This challenge can be met through the creative development of conventional energy resources alongside the development of alternative technologies. This must be aggressively pursued in two parallel paths: first, we need to become increasingly creative about finding and developing conventional energy sources, whether they be oil, gas, coal or nuclear – and do so in ways that are environmentally and socially responsible. Second, we should use these conventional sources to help drive research and development of alternative energy and new environmental technologies.

There was much discussion about reducing carbon emissions, but little said about providing energy for all and reducing poverty.

Alternative energy sources such as solar, wind, geothermal and biofuels need to constitute an increasing part of the energy mix. However, developing these alternatives is a slow process, which means hydrocarbons will continue to play a dominant and crucial role in the coming decades. Nuclear energy is not the only solution for the reduction of CO₂ emissions, but nuclear power offers an attractive alternative to other energy sources, especially hydrocarbon technologies. Therefore, nuclear energy must be accepted as a key component in a new energy mix.

Efficient and sustainable energy solutions are needed that also protect the environment, and nuclear energy needs to gain wide acceptance as a key contributor in the energy mix in the coming years. If we want to lower emissions, we have to develop energies that do not emit – and that means renewable and nuclear energies. These two types of energy are compatible, because nuclear is a constant source while most renewables are intermittent. While it is true that a nuclear power plant is expensive to construct, over the long term nuclear power is a very competitive energy source. Once on stream, power production costs are low compared to fossil fuel-burning installations, because the price of uranium is relatively stable compared to fossil fuel prices. This is an attractive feature in favour of economic growth.

In terms of the disposal of nuclear waste, recycling technology already exists. We have solutions today and we need to deploy them as soon as possible; but we need public

acceptance. We know how to recycle 96 per cent of spent fuel. The problem is the last 4 per cent. We know how to transform it into an inactive form. In Slovenia, we have already decided to build up new storage for nuclear waste near the existing nuclear power plant (NEK) at Vrbina, nearby the town of Krško.

I think and hope that Slovenia will find its way in the energy field and will decide to have a proper energy mix, particularly with the use of sustainable energy sources that include nuclear and renewable energy technologies. In the field of nuclear energy, we have 40 years of experience from the reliable and safe operation of existing nuclear power plant; this will prove to be an important asset in the future. Regarding renewable sources, we also have very good experience and knowledge of how to build, manage, operate and maintain technologies that benefit renewable energy sources. They must incorporate as many alternative technologies (solar, wind, geothermal) to be used in the available capability. Of course, in all of this, we must not forget efficient energy use to ensure we can most effectively contribute to the preservation of our environment and our only planet – Earth.

Krško, November, 2010

Andrej PREDIN

Table of Contents / Kazalo

Rain energy as a green energy source?/

Energija dežja kot zeleni vir električne energije?

Andrej Predin, Jurij Avsec, Gorazd Hren13

Generalised continuous variable dynamic linear programming in energy systems/

Zvezno variabilno dinamično linearno programiranje v energetskih sistemih

Janez Usenik19

Virial coefficients of higher orders for polar molecules/

Virialni koeficienti višjih redov za zelo polarne molekule

Jurij Avsec33

Experimental and numerical analysis of the impact of particles on the development of cavitation flow around a hydrofoil /

Eksperimentalna in numerična analiza vpliva delcev na razvoj kavitacije okoli lopatičnega profila

Matjaž Hriberšek, Andrej Predin, Boštjan Gregorc47

Failure analysis of a railway brake disc /

Analiza poškodb železniškega zavornega diska

Blaž Šamec, Grega Oder, Tone Lerher, Iztok Potrč65

Instructions for authors73

RAIN ENERGY AS A GREEN ENERGY SOURCE?

ENERGIJA DEŽJA KOT ZELENİ VIR ELEKTRIČNE ENERGIJE?

Andrej Predin¹, Jurij Avsec², Gorazd Hren³

Keywords: Green energy sources, Monsoon rain, Energy of the rain

Abstract

The paper focuses on using rain as a possible energy source in areas of monsoon rain. On the basis of physical considerations, taking into account the basic laws of mechanics, fluid mechanics and aero-dynamics, the idea of exploiting rain as a green source for energy production is developed. The energy-poor areas of Asia could take advantage of heavy rain during periods of monsoons. From the commercial point of view, this energy source is not profitable, but bearing in mind the underdevelopment of those areas, this energy source could be sufficient for primary energy supply of individual residential houses.

Povzetek

Članek se osredotoča na uporabo dežja kot možnega vira energije na področjih z monsunskim deževjem. Ideja o izkoriščanju dežja kot zelenega vira za proizvodnjo električne energije se je razvila ob upoštevanju osnovnih zakonitosti mehanike, mehanike tekočin in aerodinamike. V Aziji je veliko področij, kjer se srečujejo s pomanjkanjem energije, podvrženi pa so obdobjem obilnega monsunskega deževja, ki bi ga lahko izkoristili za izboljšanje stanja na energetskem področju. Takšen vir energije komercialno ni zanimiv, glede na obstoječe stanje pa bi lahko zadoščal za oskrbovanje individualnih stanovanjskih hiš s primarno energijo.

¹ Full Professor Andrej PREDIN, Ph.D., Faculty of Energy Technology, University of Maribor

² Associate Professor Jurij AVSEC, Ph.D., Faculty of Energy Technology, University of Maribor

³ Assistant Professor Gorazd HREN, Ph.D., Faculty of Energy Technology, University of Maribor

1 INTRODUCTION

Worldwide demand for energy is projected to increase steadily for the foreseeable future. Fortunately, there are many means of harnessing energy that have less damaging impacts on our environment and are available almost anywhere on Earth. Such alternative energy sources become an issue in the early 1970s when oil prices increased considerably and we were with supply shortage. At the present time, we are facing an ominous reality. The world’s energy needs are greater than ever before, driven by an increase of population worldwide, and the industrial and economical development of Asian countries. Furthermore, we are facing demanding and highly increased oil-based energy while the world supply is decreasing. Practically since year 2000, the world is facing permanent increase of oil prices and consequently searching the new energy resources and exploit technologies that are efficient and environmentally acceptable. Putting a price on carbon emissions and developing green energy sources are recommendations on sustainable development included in a report by Kintisch [1]. His conclusions suggest that the urgency of the problem will make up for its lack of originality in grabbing the attention of policymakers around the globe, and they intend to launch a major effort to get the message out.

As mentioned in Inter-Academy Council (IAC) report [1] in Amsterdam, the Netherlands, seven years ago, it is a moral and social imperative to meet the basic energy needs of the poorest people on this planet. That fact indicates that the developed areas of global academic community are obligated to find and develop green sustainable energy technologies that will help to mitigate basic energy needs in the poorest regions. Could the monsoon rain be such an alternative and green energy source? As Jagadis Sjukla reports in [2], there are some areas in the Indian subcontinent, or more widely in the Asia, where up to 16 mm of rain per square meter per hour were observed during monsoon periods between 2003 and 2006.

2 ENERGY ESTIMATION OF THE RAIN FLOW

The disposable energy of the rain can be practically estimated in two ways. First, the rain could be treated as a flow of the individual water drops, using classic Newtonian mechanical theory. Second, the rain could be treated as a two-phase flow and presented with Euler’s theory of a velocity field in a vertical direction, considering the earth’s gravity.

With Newton’s classic mechanical theory, the energy of water drops could be estimated. The rain drop is falling from clouds based at 2500 m above sea level (ASL) with an approximate mass of 1 gram per individual drop. When the water drop forms, it is spherical. During the fall, the drop is transformed into the more aerodynamic rain-drop shape. Because it starts with free fall, this means from the regular acceleration movement, the differential equation of such movement could be written as:

$$a = \frac{dv}{dt} = \frac{d^2s}{dt^2} = const. \tag{2.1}$$

Where V is velocity, t is time, and s is distance (path). Equation (2.1) has a solution for free fall cases, in the following form

$$V = \sqrt{2gh}, \tag{2.2}$$

in which g is the earth's acceleration coefficient (9.81 m/s^2) and h is the height from which the water drop falls.

Equation (2.2) is suitable only if the exact height (path) is known, and the air drag is neglected. In our case, the drag force is highly influential on drop velocity, and must be considered.

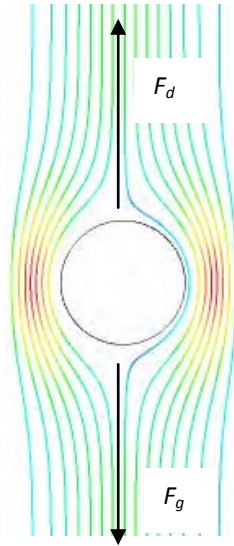


Figure 1: Forces on rain drop.

A rain drop (Figure 1), treated as a falling object, reaches terminal velocity when the downward force of gravity (F_g) equals the upward force of drag (F_d). The net force on the rain drop is zero, resulting into a constant drop velocity. Mathematically, an object, in our case rain drop, asymptotically approaches and can never reach its terminal velocity. When the object accelerates (usually downwards, due to gravity), the drag force acting on the object increases. At a particular velocity, the drag force produced will equal the object's weight (mg). Terminal velocity (also called settling velocity) varies directly with the ratio of drag to weight. Greater drag means a lower terminal velocity, while increased weight means a higher terminal velocity. The rain drop's weight directly depends on drop size that is formed at different rain types. In the case of a rain drop, it is possible that the drop is moving downward with greater than terminal velocity, because the drop usually changes its shape (into a more aerodynamic form), which is affected by a downward force or it falls from a thinner part of the atmosphere.

Mathematically, the resulting force is reached when the downward force of gravity (F_g) equals the upward force of drag (F_d), (that is valid for Reynolds numbers, i.e. $Re > 10^5$)

$$F = F_g - F_d, \tag{2.3}$$

$$F = mg - C_d A p_k, \tag{2.4}$$

where C_d is the coefficient of the air resistance (drag coefficient), A is project cross-section perpendicular to the drop direction, and p_k is kinetic flow pressure at the stagnation point on a spherical surface, m is the mass of the rain drop (object), and g is the acceleration due to

gravity. Dynamic pressure at the stagnation point on the sphere, known also as dynamic pressure, could be written as

$$p_k = \frac{1}{2}\rho V^2, \tag{2.5}$$

Where ρ is the fluid density (e.g. density of air). The terminal velocity is reached when $F = 0$, so

$$mg - p_k Ac_d = 0 = mg - \frac{1}{2}\rho V^2 Ac_d \tag{2.6}$$

Solving for V to obtain the expression for the terminal velocity, we obtain

$$V_t = \sqrt{\frac{mg}{\rho Ac_d}}. \tag{2.7}$$

With the evaluation coefficient C_d of aerodynamic resistance, considering the form of a sphere and/or drop for the $Re > 10^5$, we can calculate the terminal velocity of raindrops for different diameters, having assessed the level from which the drop could fall (reach) to the ground (without dividing). Using equation (2.7), the terminal rain drop velocity could be calculated for different drop sizes and different rain types. The results are given in the Table 1.

Table 1: Typical drop sizes and its terminal velocities, [3]

RAIN TYPE	Drop Size [mm]	Terminal Velocity [m/s]
Light Stratiform Rain (1 mm per hour)		
Small Drop	0.5	2.06
Large Drop	2.0	6.49
Moderate Stratiform Rain (6.4 mm per hour)		
Small Drop	1.0	4.03
Large Drop	2.6	7.57
Heavy Thundershower (25.4 mm per hour)		
Small Drop	1.2	4.64
Large Drop	4.0	8.83
Largest Possible Drop	5.0	9.09
Hailstone	10	10.00
Hailstone	40	20.00

The energy estimation of rain drops is presented in Table 2.

Table 2: Available energy of rain drops

RAIN TYPE	Drop Size [mm]	Available kinetic energy of one drop [J]	Available kinetic energy at m ² in one hour [J/m ² (hour)]	Available power at m ² [W]/m ²
Light Stratiform Rain (1 mm per hour)				
Small Drop	0.5	2.77E-07	4.24	0.0012
Large Drop	2.0	1.76E-04	42.08	0.0117
Moderate Stratiform Rain (6.4 mm per hour)				
Small Drop	1.0	8.50E-06	103.84	0.1844
Large Drop	2.6	5.27E-04	366.38	0.6507
Heavy Thundershower (25.4 mm per hour)				
Small Drop	1.2	1.95E-05	546.30	3.8506
Large Drop	4.0	2.61E-03	1978.43	13.9450
Largest Possible Drop	5.0	5.40E-03	2096.65	14.7783

If we considered Jagadis Sjukla's report, [2], there are some areas in India or widely in Asia where up to 16 mm of water per square meter per hour were observed during monsoon season, which corresponds between "Moderate Stratiform Rain" and "Heavy Thundershower" with large drops (Table 1). This means that approximately 10 W of power per square meter is available, in such regions during monsoon rain. If we compare this estimation with wind energy potential, then this energy source is very low from a commercial point of view. Regardless, some small buildings could be adopted with wind turbines. A wind turbine with diameter of 15 m, with efficiency of approximately 0.4, could produce approximately 0.8 kW. This power installation could fulfill the basic household energy needs for lightening and simple heating systems during the long and dark days of monsoon rains.

3 CONCLUSION

With efforts to maximize the use of renewable energy sources, the idea of exploiting the energy of monsoon rain is interesting, especially as an independent and widespread source. The fundamental problem of minimum energy supply could be solved locally in monsoon areas. Presently available technology would be very affordable and suitable to use in economically poor, monsoon area of Asia. With appropriate international support, it would be possible to provide to the local population with enough energy for basic needs such as lighting and heating homes.

References

- [1] **Eli Kintisch:** *Energy policy: National Academies Make Case for Sustainable Growth*. (With reporting by Richard Stone in Beijing), *SCIENCE*, VOL 318, 26 October 2007, p. 547.
- [2] **Jagadish Shukla:** *Atmosphere: Monsoon Mysteries*. *SCIENCE*, VOL 318, 12 October 2007, p.p. 204 -205.
- [3] <http://www.shorstmeyer.com/wxfags/float/rdtable.html> (Sources: R.R. Rogers, *A Short Course in Cloud Physics*, 2 ed. Pergamon Press, 1979, H. Byers, *General Meteorology*, 3 ed. McGraw-Hill, 1959, H.R. Pruppacher, *Microstructure of Atmospheric Clouds and Precipitation in Clouds: Their Formation, Optical Properties and Effects*, P. Hobbs and A. Deepak, eds., Academic Press, 1981.), Access date: April, 5 2010.

GENERALISED CONTINUOUS VARIABLE DYNAMIC LINEAR PROGRAMMING IN ENERGY SYSTEMS

ZVEZNO VARIABILNO DINAMIČNO LINEARNO PROGRAMIRANJE V ENERGETSKIH SISTEMIH

Janez Usenik[✉]

Keywords: linear programming, dynamic model, convex link, optimising, energy system.

Abstract

This article presents an algorithm for the modification of continuous dynamic linear programming: all elements in matrix A are functions of time and are divided into two parts, i.e. submatrixes. In the first submatrix, all the elements are finite functions known in advance; in the second one, the elements are, however, unknown but linked convexly in columns. The task is to find the optimum of objective/criterion function and (at the same time) to determine the optimum structure of unknown variable columns. This means that, according to the meaning of the elements of matrix A in actual practice, in a wider sense the described method represents an important aid in practical models. One of the possibilities is optimising the control of energy systems.

Povzetek

V članku je predstavljena modifikacija zveznega dinamičnega linearnega programa, ki omogoča naslednje možnosti: vsi elementi matrike sistema A so časovne funkcije in so razdeljeni v dve delni matriki. V prvi delni matriki so vsi elementi končne in vnaprej znane funkcije, v drugi delni

[✉] Corresponding author: Prof. Janez Usenik, PhD, University of Maribor, Faculty of Energy Technology, Tel.: +386 31 751 203, Fax: +386 7 620 2222, Mailing address: Hočevarjev trg 1, 8270 Krško, Slovenia, e-mail address: janez.usenik@uni-mb.si

matriki pa so elementi neznane funkcije, vendar pa so po stolpcih konveksno zavezani. Naloga je poiskati optimum namenske funkcije, hkrati s tem pa tudi določiti optimalno strukturo neznanih variabilnih stolpcev. To pomeni, da glede na vsebinski pomen elementov matrike A v konkretnih primerih novi algoritem odpira različne nove poglede na optimiranje v praktičnih modelih. Ena od takšnih možnosti je vsekakor optimiranje procesov v upravljanju energetskih sistemov.

1 INTRODUCTION

In the problem of linear programming (LP) in the general form, Dantzig [1]

$$\begin{aligned} &opt(c, x) \\ &Ax = b \\ &x \geq 0 \end{aligned}$$

we make two modifications consecutively:

First, we can change all constant vectors by vector functions in a finite interval of time $[0, T]$, $T < \infty$ so that $b(t) \in R_b$, $c(t) \in R_c$, $x(t) \in R_x$, $A(t) \in R_A$. The functions from R_b, R_c and R_A are continuous and at least once-derived real functions. Functions from R_b are still non-negative and functions from R_A are monotonously limited and only finitely many times non-finite real functions. With these completions, we have now the problem called *Continuous Variable Dynamic Linear Programme (c/b/A-CDLP)*, Rupnik [2]:

$$\begin{aligned} &opt[c(t), x(t)] \\ &A(t)x(t) = b(t) \\ &x(t) \geq 0 \end{aligned} \tag{1.1}$$

Second, we divide the matrix $A(t)$ into two parts $A(t) = [A_0(t); \tilde{A}(t)]$. All the elements of the first submatrix $A_0(t)$ are known finite real functions, whereas all the elements of the second submatrix $\tilde{A}(t) = [\hat{p}_{\mu+1}(t) \ \hat{p}_{\mu+2}(t) \ \dots \ \hat{p}_n(t)]$ are unknown finite real functions but convexly linked in columns $\hat{p}_j(t) \in C_j(t)$ for all $j = \mu+1, \mu+2, \dots, n$. In this case, we arrive at the problem called *Generalised Continuous Variable Dynamic Linear Programming (G-c/b/A-CDLP)*, Usenik [3], [4]:

$$\begin{aligned} &opt[c(t), x(t)] \\ &[A_0(t); \tilde{A}(t)]x(t) = b(t) \\ &x(t) \geq 0 \\ &\hat{p}_j(t) \in C_j(t) \quad j = \mu+1, \mu+2, \dots, n \end{aligned} \tag{1.2}$$

2 WORKING OUT THE PROBLEM

If we omit all the variable columns in (1.2) of the matrix $A(t)$, we obtain a special case, which is identical to problem (1.1). Problem (1.2) can therefore be solved in two phases. During phase 1, we are calculating the problem:

$$\begin{aligned} & \text{opt}[c(t), x(t)] \\ & A_0(t)x(t) = b(t) \\ & x(t) \geq 0 \end{aligned} \tag{2.1}$$

Problem (2.1) is obviously c/b/A-CDLP. To set up the algorithm and prove the existence of the solution as well as the optimum method of calculating this problem, we use a step-by-step approach and calculate the following three sub-problems ($t \in [0, T]$, $T < \infty$), which are solved in Rupnik, [2]:

b-CDLP

$$\begin{aligned} & \text{opt}[c(0), x(t)] \\ & A(0)x(t) = b(t) \\ & x(t) \geq 0 \end{aligned} \tag{2.2}$$

c-CDLP

$$\begin{aligned} & \text{opt}[c(t), x(t)] \\ & A(t)x(t) = b(0) \\ & x(t) \geq 0 \end{aligned} \tag{2.3}$$

c/b-CDLP

$$\begin{aligned} & \text{opt}[c(t), x(t)] \\ & A(0)x(t) = b(t) \\ & x(t) \geq 0 \end{aligned} \tag{2.4}$$

If we mark the union of areas of admissibility of k-th solution with M_k , and the union of areas of structural constancy of the base of k-th solution with $[SS]_k$, we can prove, Usenik [3]:

Theorem 1: *If the following conditions are fulfilled: $b_{\substack{(0) \\ \{\tau_0\}, S_{\{\tau_0\}}^{(0)}}}(t) \geq 0$, $a_{\substack{(\rho-1) \\ i, S_{\{\tau_{p-1}\}}^{(\rho-1)}}}(t) > 0$, $\bar{c}_j^{(\rho-1)}(t) < 0$ for at least one $i \in \{1, 2, \dots, m\}$ and at least one monobasic $j = S_{\{\tau_{p-1}\}}^{(\rho-1)}$, $p = 1, 2, \dots, k$ then for the problem (4) i.e. c/b/A-CDLP in the non-empty area $M_k \cap [SS]_k$ one segmentally structurally stationary feasible basic solution $x^{(k)}(t) \in R_b$ exists.*

Under conditions of theorem 1, we can always obtain the optimum structurally stationary basic solution $x^{k_0(t)}$ of problem (1.1). In further study of the basic problem, we discover that the above solution of the problem of the generalised c/b/A-CDLP is only one of the several feasible basic solutions defined in the separate subinterval $\delta_{\tau_{k_0}}^{k_0}$ of basic interval $[0, T]$. For the basic problem (1.2), this solution is structurally stationary but certainly not yet optimum. In the second phase, the calculation ought to be improved, and we achieve this by additional optimisation of the structure of vectors $\hat{P}_j(t)$, $j = \mu + 1, \mu + 1, \dots, n$ under convex restriction; in this way, we manage to obtain the optimum solution of the basic problem (1.2), which is in general algorithmic structure now called *the main programme*.

The optimum solution of phase 1 (c/b/A-CDLP) is defined as the initially feasible solution of the problem (1.2) $(1)x^{(k_0)}(t) = (2)x^{(0)}(t)$ in separate subintervals $\delta_{\tau_{k_0}}^{(k_0)}$ into which the basic interval $[0, T]$ broke up during the calculations of phase 1. From this initial solution, we calculate the first feasible basic solution of the second phase $(2)x^{(1)}(t)$ as structurally stationary for separate time intervals, then the second one, the third one etc.

Suppose we got a structurally stationary feasible basic solution $(2)x^{(k-1)}(t)$ in all subintervals $\zeta_i^{(k-1)}$.

A structurally stationary constant basis $L^{\wedge(k-1)}(t)$ and its corresponding inverse $[L^{\wedge(k-1)}(t)]^{-1}$ belong to the above solution in separate subintervals. In the inverse of this basis, elements in the last line are the simplex multipliers:

$$\begin{aligned} (i)\pi^{(k-1)}(t) &= \left[-{}^{(i)}\pi_1^{(k-1)}(t) \quad -{}^{(i)}\pi_2^{(k-1)}(t) \quad \dots \quad -{}^{(i)}\pi_m^{(k-1)}(t) \ ; \ 1 \right] \\ i &= 1, 2, \dots, p_{k-1} \end{aligned} \tag{2.5}$$

By definition of simplex method, in Dantzig [1], we have

$$\begin{aligned} (i)\hat{\pi}^{(k-1)}(t) \cdot \hat{P}_j(t) &\geq 0 \quad \text{for } j = 1, 2, \dots, \mu \\ (i)\hat{\pi}^{(k-1)}(t) \cdot \hat{P}_j(t) &= 0 \quad \text{for basic index } j \in \{1, 2, \dots, n\} \end{aligned} \tag{2.6}$$

$$(i)\hat{\pi}^{(k-1)}(t) \hat{P}_0(t) = 1 \tag{2.7}$$

$$\begin{aligned} (i)\hat{\pi}^{(k-1)}(t) \hat{P}_j(t) &< 0 \quad \text{for nonbasic index } j \in \{\mu + 1, \mu + 2, \dots, n\} \\ t &\in \zeta_i^{(k-1)} \\ i &= 1, 2, \dots, p_{k-1} \end{aligned} \tag{2.8}$$

and therefore the k-th solution is derived from (k-1)-th solution if we manage to solve the system of k-th subprogrammes in all the subintervals $\zeta_i^{(k-1)}$, $i = 1, 2, \dots, p_{k-1}$:

$$\begin{aligned} & \min^{(i)} \hat{\pi}^{(k-1)}(t) \cdot \hat{p}_j^{(k-1)}(t) \\ & \hat{p}_j^{(k-1)}(t) \in C_j \\ & j \in \{1, 2, \dots, n\} \setminus I_2 \end{aligned} \quad (2.9)$$

$$\begin{aligned} & \min^{(i)} \hat{\pi}^{(k-1)}(t) \cdot \hat{Q}_{s_j}^{(k)}(t) \\ & \hat{Q}_{s_j}^{(k)}(t) \in C_{s_j}(t) \\ & s_j \in I_2 \\ & t \in \zeta_i^{(k-1)}; i = 1, 2, \dots, p_{k-1} \end{aligned} \quad (2.10)$$

As the complex polyhedrons are defined by the system

$$\begin{aligned} & \sum_{i=1}^{m+1} \alpha_{ijk} \cdot \tilde{a}_{ij}(t) \leq d_{jk}(t) \\ & j = \mu + 1, \mu + 1, \dots, n \\ & k = 1, 2, \dots, p_j \end{aligned} \quad (2.11)$$

then (2.9) represents system c/b-CDLP if the following is true

$$\begin{aligned} & d(t) \in R_b \\ & d(t) \geq 0 \\ & {}^{(i)} \hat{\pi}^{(k-1)}(t) \in R_c \\ & \tilde{a}_{ij}(t) \in X \end{aligned} \quad (2.12)$$

3 THE EXISTENCE OF THE SOLUTION AND OPTIMAL SOLUTION

In Usenik, [3] the next theorem is proved:

Theorem 2: For $c_j^{(0)}(t) \in R_c$ and strictly positive elements $a_{\substack{r, \rho-1 \\ \{r, \rho-1\}}}^{(p-1), s_r^{(p)}}(t) \in R_A, p=1, 2, \dots, k_0$ calculating c/b/A-CDLP and for strictly positive $\tilde{a}_{r, s_q}^{(q-1)}(t), q=1, 2, \dots, k$ the system of q-th subprograms are the problems of the c/b-CDLP type.

From Theorem 2, we can see that further subdivision of subinterval $\zeta_i^{(k-1)}$ takes place. In general, during the process of calculating r-th c/b-CDLP the h-th subinterval can break up into subintervals ${}_{(r)}\Delta_{h,1}^{(k-1)}, {}_{(r)}\Delta_{h,2}^{(k-1)}, \dots, {}_{(r)}\Delta_{h,\rho_h}^{(k-1)}$ with the following solutions:

$$\begin{aligned} {}^{(h)}\pi^{(k-1)}(t) \cdot \hat{P}_{r,1}^{(k)}(t) &\in {}_{(r)}\Delta_{h,1}^{(k-1)} \\ {}^{(h)}\pi^{(k-1)}(t) \cdot \hat{P}_{r,2}^{(k)}(t) &\in {}_{(r)}\Delta_{h,2}^{(k-1)} \\ &\dots \\ {}^{(h)}\pi^{(k-1)}(t) \cdot \hat{P}_{r,\rho_k}^{(k)}(t) &\in {}_{(r)}\Delta_{h,\rho_k}^{(k-1)} \end{aligned} \tag{3.1}$$

For the purpose of further optimisation in the main programme, these solutions must be negative.

Theorem 3: Under conditions for the existence of optimum solution c/b/A-CDLP and under conditions of theorem 2, there is k-th feasible basic solution which is structurally stationary in separate subintervals of the ${}_{(r)}\Delta_{h,1}^{(k-1)}, {}_{(r)}\Delta_{h,2}^{(k-1)}, \dots, {}_{(r)}\Delta_{h,\rho_h}^{(k-1)}$ type.

During further subdivision of subintervals $\zeta_i^{(k-1)}, i=1, 2, \dots, \rho_{k-1}$, subintervals ${}_{(z)}\Delta_{i,\rho_k}^{(k-1)}, z=1, 2, \dots, n-\mu$ are generally not the same. For this reason, separate solutions are compared by means of the definite integral in every $\zeta_i^{(k-1)}$ by establishing the criterion for the selection of the input vector into the basis of the main programme:

$$\min_j \left[\sum_{i=1}^{K_k} \int_{t_{i-1}}^{t_i} {}^{(h)}\pi^{(k-1)}(t) \cdot \hat{P}_{j,i}^{(k)}(t) dt \right], j \in \{\mu+1, \mu+2, \dots, n\} \tag{3.2}$$

As the solution of k-th subprogrammes for $t \in \zeta_i^{(k-1)}$ must be monotonous, we introduce other additional conditions (3.2). When we have monotonously selected the index of the input vector for the main programme, there are two possibilities:

1. The minimum of the average solution in the entire $\zeta_i^{(k-1)}, i=1, 2, \dots, \rho_{k-1}$, is the one with the index s_k while the vector with this index is not yet in the basis. In this case, the vector $\hat{P}_{s_k}^{(k)}(t)$

enters the basis at $\zeta_i^{(k-1)}$. As it is possible that the convex polyhedron $C_{s_k}(t)$ may not have been completely exploited, we have to make an allowance for the variation of this vector:

$$\begin{aligned} \hat{P}_{s_k}(t) &= \left[\hat{P}_{s_k}^{(k)}(t) \cdot {}_{(k)}x_{s_k}(t) \cdot \hat{Q}_{s_k}^{(k+1)}(t) \cdot {}_{(k+1)}x_{s_k}(t) \right] \cdot \frac{1}{x_{s_k}(t)} \\ x_{s_k}(t) &= {}_{(k)}x_{s_k}(t) + {}_{(k+1)}x_{s_k}(t), \quad t \in {}_{(s_k)}\Delta_{i,j}^{(k-1)}, i \in \{1, 2, \dots, p_{k-1}\} \\ \bigcup_{j=1}^{\sigma_k} {}_{(s_k)}\Delta_{i,j}^{(k-1)} &\subseteq \zeta_i^{(k-1)} \end{aligned} \quad (3.3)$$

In this way, we obtain a *modified main programme of k-th grade* of c/b-CDLP type for each subinterval ${}_{(s_k)}\Delta_{i,j}^{(k-1)}, j = 1, 2, \dots, \sigma_k$.

2. The minimum of the average solution is the one with the index s_k while the vector with this index was already in the basis earlier. In this case, the vector $\hat{P}_{s_j}^{(k)}(t)$ in the interval $\zeta_i^{(k-1)}$ fulfilling the conditions of optimality again enters the basis. We have to consider the possibility that the convex polyhedron $C_{s_k}(t)$ may not yet have been exploited to the full, so we again have to make allowance for the variation in it. Thus we obtain a modified main programme of k-th grade for each subinterval ${}_{(s_k)}\Delta_{i,j}^{(k-1)}$ similar to programme (7) and we calculate it in the same way.

Now the following it is true: programme c/b/A - CDLP, which represents phase 1 of working out the solution to programme (1.2), has a finite number of iteration steps (Theorem 1); under conditions of Theorem 2, separate subprogrammes are all type c/b-CDLP and also have a finite number of iteration steps; the vectors $\hat{P}_j(t)$ are either extreme points of convex polyhedrons or a linear combination of these points. If convex polyhedrons have a finite number of extreme points, we can see that in this case the number of iteration steps is finite.

Theorem 4: *If the following conditions are fulfilled*

1. *for the existence of the optimum solution c/b/A-CDLP the conditions of theorem 1,*
2. *elements $a_{r_{\tau_{p-1}}^{(p-1)}, s_{\tau_p}^{(p)}}(t) \in R_A$ are strictly positive for $p = 1, 2, \dots, k_0$,*
3. *convex polyhedrons have a finite number of extreme points,*
4. $c_j^{(0)}(t) \in R_c$

then there is an optimum solution of the problem G - c/b/A CDLP (2) in a non-empty segment of the interval.

4 NUMERICAL EXAMPLE

Calculate problem (2) for $t \in [0, 2.5]$ if vector and matrix functions are the following:

$$c(t) = [2 + 2t \quad 6 + 2t \quad 8 + 2t \quad 5 + 2t]$$

$$b(t) = \begin{bmatrix} 80 - 5t \\ 40 + 15t \\ 120 - 20t \end{bmatrix}$$

$$A(t) = [A_0(t) : \tilde{A}(t)] = \begin{bmatrix} 4 & 1 + 2t & 2 + 3t & 2 & \tilde{a}_{15}(t) & \tilde{a}_{16}(t) \\ 2 + t & 5 & 0 & 4 + t & \tilde{a}_{25}(t) & \tilde{a}_{26}(t) \\ 0 & 2 & 4 & 1 + t & \tilde{a}_{35}(t) & \tilde{a}_{36}(t) \end{bmatrix}$$

$$\hat{p}_5(t) = \begin{bmatrix} \tilde{a}_{15}(t) \\ \tilde{a}_{25}(t) \\ \tilde{a}_{35}(t) \end{bmatrix} \in C_5(t)$$

$$C_5(t) : \begin{cases} 3\tilde{a}_{15}(t) + 3\tilde{a}_{25}(t) + 3\tilde{a}_{35}(t) - (3 + 3t)\tilde{a}_{45}(t) = 9 + 3t \\ 2\tilde{a}_{15}(t) + (5 + t)\tilde{a}_{25}(t) + \tilde{a}_{35}(t) + 3\tilde{a}_{45}(t) = 10 + 2t \end{cases}$$

$$\hat{p}_6(t) = \begin{bmatrix} \tilde{a}_{16}(t) \\ \tilde{a}_{26}(t) \\ \tilde{a}_{36}(t) \end{bmatrix} \in C_6(t) \quad C_6(t) : \begin{cases} (2 + t)\tilde{a}_{65}(t) + \tilde{a}_{26}(t) + \tilde{a}_{36}(t) + 2\tilde{a}_{46}(t) = 6 + 3t \\ 4\tilde{a}_{16}(t) + 2\tilde{a}_{26}(t) + 2\tilde{a}_{36}(t) - (4 + 2t)\tilde{a}_{46}(t) = 8 + 4t \end{cases}$$

According to the given algorithm, we have two phases. In phase 1 of calculating (c/b/A-CDLP), different optimum solutions appear in the following subintervals (Fig. 1): $[0, 0.233)$, $[0.233, 0.693)$, $[0.693, 2.0)$, $[2.0, 2.2)$ and $[2.2, 2.5]$. In the second phase, we have to define the optimum of the criterion function and simultaneously determine the optimum structure of unknown convexly linked columns. We can obtain the optimal structurally stationary feasible basic solution in separate intervals.

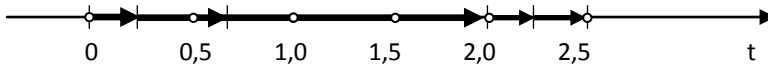


Figure 1: Time interval $[0, 2.5]$ and its subintervals

The solution G-c/b/A-CDLP in these subintervals is the following.

A) the first subinterval $[0, 0.233)$:

$$x_{opt}(t) = \begin{bmatrix} x_1(t) \\ x_6(t) \\ x_5(t) \end{bmatrix} = \begin{bmatrix} \frac{40+15t}{2+t} \\ \frac{480+40t-20t^2}{20+16t+3t^2} \\ \frac{50-5t^2-10t^3}{38+48t+19t^2+2t^3} \end{bmatrix}$$

$$z_{min}(t) = \frac{39520 + 105720t + 112760t^2 + 62170t^3 + 18780t^4 + 2930t^5 + 180t^6}{(2+t)(20+16t+3t^2)(19+15t+2t^2)}$$

$$\hat{p}_5(t) = \hat{p}_5^{(2)}(t) = \begin{bmatrix} \frac{19+15t+2t^2}{5+2t} \\ 0 \\ 0 \\ 4 \\ \frac{4}{5+2t} \end{bmatrix} \quad \hat{p}_6(t) = \hat{p}_6^{(1)}(t) = \begin{bmatrix} 0 \\ 0 \\ \frac{20+16t+3t^2}{4+t} \\ \frac{2+t}{4+t} \end{bmatrix}$$

B) the subinterval $[0.233, 0.693)$:

$$x_{opt}(t) = \begin{bmatrix} x_2(t) \\ x_5(t) \\ x_6(t) \end{bmatrix} = \begin{bmatrix} \frac{40+15t}{5} \\ \frac{360+24t-78t^2-12t^3}{19+15t+2t^2} \\ \frac{416-26t^2}{20+16t+3t^2} \end{bmatrix}$$

$$z_{min}(t) = \frac{27952 + 48708t + 38542t^2 + 17820t^3 + 4804t^4 + 666t^5 + 36t^6}{(20+16t+3t^2)(19+15t+2t^2)}$$

$$\hat{p}_5(t) = \hat{p}_5^{(2)}(t) = \begin{bmatrix} \frac{19 + 15t + 2t^2}{5 + 2t} \\ 0 \\ 0 \\ \frac{4}{5 + 2t} \end{bmatrix}$$

$$\hat{p}_6(t) = \hat{p}_6^{(1)}(t) = \begin{bmatrix} 0 \\ 0 \\ \frac{20 + 16t + 3t^2}{4 + t} \\ \frac{2 + t}{4 + t} \end{bmatrix}$$

C) the subinterval [0.693, 2.0) and [2.0, 2.2):

$$x_{opt}(t) = \begin{bmatrix} x_4(t) \\ x_5(t) \\ x_6(t) \end{bmatrix} = \begin{bmatrix} \frac{40 + 15t}{4 + t} \\ \frac{1200 + 630t + 35t^2 - 10t^3}{(4 + t)(19 + 15t + 2t^2)} \\ \frac{880 + 1290t - 115t^2 - 105t^3}{(2 + 3t)(20 + 16t + 3t^2)} \end{bmatrix}$$

$$z_{min}(t) = \frac{111920 + 237650t + 183115t^2 + 84675t^3 + 22490t^4 + 3170t^5 + 180t^6}{(4 + t)(20 + 16t + 3t^2)(19 + 15t + 2t^2)}$$

$$\hat{p}_5(t) = \hat{p}_5^{(2)}(t) = \begin{bmatrix} \frac{19 + 15t + 2t^2}{5 + 2t} \\ 0 \\ 0 \\ \frac{4}{5 + 2t} \end{bmatrix}$$

$$\hat{p}_6(t) = \hat{p}_6^{(1)}(t) = \begin{bmatrix} 0 \\ 0 \\ \frac{20+16t+3t^2}{4+t} \\ \frac{2+t}{4+t} \end{bmatrix}$$

D) the subinterval [2.2, 2.5]:

$$x_{opt}(t) = \begin{bmatrix} x_3(t) \\ x_6(t) \end{bmatrix} = \begin{bmatrix} \frac{80-5t}{2+3t} \\ \frac{1960+430t^2-15t^3}{(2+3t)(20+16t+3t^2)} \end{bmatrix}$$

$$\begin{aligned} x_6(t) &= x_6^{(1)}(t) + x_6^{(2)}(t) = \frac{-320+1280t-100t^2-60t^3}{(2+3t)(20+16t+3t^2)} + \frac{160+100t+15t^2}{(20+16t+3t^2)} = \\ &= \frac{1960t+230t^2-15t^3}{(2+3t)(20+16t+3t^2)} \end{aligned}$$

Because

$$x_6(t)\hat{p}_6(t) = x_6^{(1)}(t)\hat{p}_6^{(1)}(t) + x_6^{(2)}(t)\hat{p}_6^{(2)}(t)$$

and

$$\hat{p}_5(t) = \hat{p}_5^{(2)}(t) = \begin{bmatrix} \frac{19+15t+2t^2}{5+2t} \\ 5+2t \\ 0 \\ 0 \\ \frac{4}{5+2t} \end{bmatrix}$$

we have

$$\hat{P}_6(t) = \begin{bmatrix} 0 \\ \frac{(2+3t)(40+15t)(20+16t+3t^2)}{1960t+430t^2-15t^3} \\ \frac{(-80+340t-60t^2)(20+16t+3t^2)}{1960t+430t^2-15t^3} \\ \frac{2+t}{4+t} \end{bmatrix}$$

In real situations, such as a task to optimise energy capacities for permanent and reliable electricity supply (Fabijan, Predin, [5]), “time interval” $[0, T]$ means the interval of prediction some parameters (quantity, price, capacities etc.). In the example above, time interval $[0, 2.5]$ could be given in different time unit: weeks, months or years. If the interval $[0, 2.5]$ means 10 years, i.e. $[0, 10 \text{ years}]$, then subintervals in our example are, in years: $[0, 0.233] \equiv [0, 0.93]$, $[0.233, 0.693] \equiv [0.93, 2.77]$, $[0.693, 2.2] \equiv [2.77, 8.8]$ and $[2.2, 2.5] \equiv [8.8, 10]$.

5 CONCLUSION

From a short description of the procedure, we can see that the problem that we set up at the beginning can be solved and also applied in concrete situations.

Study of problem (1.2) raises questions that will be the subject of further research.

Interval $[0, T]$ over which functions $x(t), b(t), c(t)$ and $A(t) = [a_{ij}(t)]_{m \times n}$ have been defined and with them we have been calculating G-c/b/A-CDLP (2) continually; as a rule, we break into more subintervals in the process of working out the problem. The union of these intervals is smaller or at least the same as the initial interval. It may therefore occur that in some cases that depend on the form of vector functions, the initial finite interval $[0, T]$ breaks into quite a large number of non-empty subintervals. In such cases, theoretically optimal solutions in to short time intervals cannot give optimum results in practical application. This is the reason research is directed towards defining additional limiting conditions that will help alleviate this problem.

Because of the possibility of application of the theory of systems in solving concrete problems in the field of optimisation, further research will emphasise the introduction of the results of generalised c/b/A-CDLP in this sphere. In this sense, there are great possibilities in solving primarily system problems in different variations. It is obvious that some new limitations will have to be set up; new conditions will also be introduced because of the transformation of real vector functions into the zone of complex functions.

References

- [1] **Dantzig, G.B.:** *Linear Programming Extensions*, Princeton University Press, 1996.
- [2] **Rupnik, V.:** *Zvezno dinamično linearno programiranje*, Založba Obzorja Maribor, 1978.
- [3] **Usenik, J.:** *Generalizirano zvezno variabilno dinamično linearno programiranje*, Univerza v Ljubljani, 1983.
- [4] **Usenik, J.:** *Generalized Continuous Variable Dynamic Linear Programming (G-c/b/A-CDLP)*, Some selected papers, University of Ljubljana, 1997.
- [5] **Fabijan, D., Predin, A.:** *Optimal energy capacities and technologies for permanent and reliable electricity supply, considering risk control*, JET Journal of Energy Technology, Volume 2 (2009), p.p. 69–84.

VIRIAL COEFFICIENTS OF HIGHER ORDERS FOR POLAR MOLECULES

VIRIALNI KOEFICIENTI VIŠJIH REDOV ZA ZELO POLARNE MOLEKULE

Jurij Avsec^{3†}

Keywords: thermo-physical properties, virial equation, statistical mechanics

Abstract

This paper features a mathematical model for computing the second, third virial coefficient and higher orders of virial coefficients for polar fluids on the basis of statistical mechanics. The model for the calculation of equilibrium thermodynamic properties contains all important molecular contributions (translation, rotation, internal rotation, vibration, intermolecular potential energy and the influence of electron and nuclei excitation). The constants necessary for the computation, such as the characteristic temperatures of rotation, electronic state and the inertia moments, are obtained analytically by applying the knowledge of the atomic structure of the molecule. The vibration constants are obtained using the modified Urey-Bradley force field. In this paper we have developed a new model for the calculation of the second virial coefficient that yields favourable results in practical computations for a large number of components and within a relatively wide range of densities and temperatures. We consider rigid nonlinear molecules with the reference of the Lennard-Jones interaction potential and dipole moment as the basis of mean field theory. The constants necessary for computation, such as the characteristic temperatures of rotation, electronic state and the inertia moments, are obtained analytically by applying the knowledge of the atomic structure of the molecule. The model presented is the original part of this work and is new to the field of thermodynamics.

^{3†} Assoc. Prof. Jurij Avsec, , Tel.: +386-7-620-2217, Fax: +386-2-620-2222, Mailing address: University of Maribor, Faculty of Energy Technology, Hočevanje trg 1, SI-8270 Krško, SLOVENIA, E-mail address: jurij.avsec@uni-mb.si

There are several methods for computing the influence of anisotropic potentials. In this paper, the Lucas-Gubbins model was used, which yields favourable results in practical computations for a large number of components and within a relatively wide range of densities and temperatures. We consider rigid nonlinear molecules with the assumption that all anisotropic interactions are scalars. The multipole expansion is terminated at the octopole term. Intermolecular repulsion interaction is modelled by the Lennard-Jones r^{-12} law. The induction interactions are formulated with the isotropic polarizability approximation. Intermolecular interactions are limited to the third-order term; cross terms between intermolecular interactions are not considered. In this paper, models will be presented obtained on basis of the pure theory (hard sphere, Lennard-Jones etc.) from the Chapman-Enskog theory and as well as on the basis of the background functions for the transport properties for pure fluids. These functions are presented as general equations in the form for the temperature-dependent dilute gas contributions and the terms for the temperature and density dependent excess contributions. The analytical results obtained with non-equilibrium statistical thermodynamics are compared with experimental data and empirical equations on the basis of experimental results. The analytical results for the viscosity are again compared with the experimental data obtained with dynamic light scattering and the agreement was found to be very good.

Povzetek

V predstavljenem članku je obravnavan model izračuna virialnih koeficientov. V članku je prikazana primerjava izračunov dobljenih s pomočjo statistične termodinamike. Za izračun termodinamičnih veličin stanja s pomočjo statistične termodinamike so upoštevani vplivi rotacije, translacije, notranje rotacije, vibracije atomov oz. skupin atomov. Vpliv medmolekularnega potenciala je zajet s pomočjo perturbacijske metode. Matematični model omogoča izračun tako v podkritičnem kot v nadkritičnem območju za enofazne sisteme.

1 INTRODUCTION

Virial coefficients are very important for the description of the behaviour of the equation of state (EOS). The equation of state that consists of virial coefficients often reproduces well the properties of a fluid at relatively high density as well as remaining accurate at low density. The mentioned EOS is likely to be reasonably good for most of the applications.[1]

In principle, it is possible to calculate second virial coefficients in different ways.

- A. Analytical calculation of virial coefficients from statistical mechanics.[2,3] From the theory of statistical mechanics, it is possible to calculate second, third and higher orders of virial coefficients on the basis of intermolecular potential. When the intermolecular potential is known, it is possible to calculate virial coefficients. In that case, the virial coefficients can be determined by evaluating integrals over the cluster of molecules. Unfortunately, in practice, it is very difficult to solve and obtain the analytical function of the multipolar part for higher orders of virial coefficients.
- B. Calculation of the second and higher order of virial coefficients from EOS. It is possible to calculate virial coefficients from EOS obtained on the basis of statistical mechanics or classical thermo-dynamics. In engineering practice, in most cases, the thermodynamic tables or diagrams or different empirical functions obtained from measurement are used (classical thermodynamics). Today, there are numerous

equations of state (EOS) reported in the literature for describing the behaviour of fluids: Van der Waals EOS (VDW), Peng-Robinson EOS (PR), Redlich-Kwong EOS (RK), Soave EOS etc.[4] However, these equations have exhibited some noticeable defects, such as poor agreement with experimental data at moderate densities. On the other side, we can use the complex equations of state with many constants (Benedict-Webb-Rubin (BWR) EOS, Lee-Kessler EOS, Benedict-Webb-Rubin-Starling-Nishiumi EOS (BWRSN), Jacobsen-Stewart EOS (JS), Tillner-Roth-Watanabe-Wagner EOS (TRWW), Jacobsen-Lemmon EOS (JL) etc.).[5,6]. These equations are more complicated. They have no insight into the microstructure of matter and poor agreement with experimental data outside the interpolation limits.

- C. Some researchers have extremely accurate measuring equipment for determining the second and third virial coefficient. On the basis of experimental data, it is possible to fit the constants in empirical equations.

2 COMPUTATION OF THERMODYNAMIC PROPERTIES OF THE STATE

To calculate thermodynamic functions of state, we applied the canonical partition function.[7,8] Utilising the semi-classical formulation for the purpose of the canonical ensemble for the N indistinguishable molecules, the partition function Z can be expressed as follows:

$$Z = \frac{1}{N!h^{Nf}} \int \dots \int \exp\left(-\frac{H}{kT}\right) \cdot d\vec{r}_1 d\vec{r}_2 \dots d\vec{r}_N d\vec{p}_1 d\vec{p}_2 \dots d\vec{p}_N \quad (2.1)$$

where f stands for the number of degrees of freedom of an individual molecule, H designates the Hamiltonian molecule system, vectors $\vec{r}_1, \vec{r}_2, \dots, \vec{r}_N$ describe the positions of N molecules and $\vec{p}_1, \vec{p}_2, \dots, \vec{p}_N$ momenta, k is the Boltzmann's constant and h is Planck's constant. The canonical ensemble of partition function for the system of N molecules can be expressed by:

$$Z = Z_0 Z_{\text{trans}} Z_{\text{vib}} Z_{\text{rot}} Z_{\text{ir}} Z_{\text{el}} Z_{\text{nuc}} Z_{\text{conf}} \quad (2.2)$$

Thus, the partition function Z is a product of terms of the ground state (0), the translation (trans), the vibration (vib), the rotation (rot), the internal rotation (ir), the influence of electrons excitation (el), the influence of nuclei excitation (nuc) and the influence of the intermolecular potential energy (conf).

Utilising the canonical theory for computation, the thermodynamic functions of the state can be defined as follows:[7]

$$\text{Pressure } p_p = kT \left(\frac{\partial \ln Z}{\partial T} \right)_V, \quad \text{Internal energy } U = kT^2 \left(\frac{\partial \ln Z}{\partial T} \right)_V,$$

$$\text{Free energy } A = -kT \cdot \ln Z, \quad \text{Entropy } S = k \left[\ln Z + T \left(\frac{\partial \ln Z}{\partial T} \right)_V \right], \quad (2.3)$$

$$\text{Free enthalpy } G = -kT \left[\ln Z - V \left(\frac{\partial \ln Z}{\partial T} \right)_V \right], \text{ Enthalpy } H_h = kT \left[T \left(\frac{\partial \ln Z}{\partial T} \right)_V + V \left(\frac{\partial \ln Z}{\partial V} \right)_T \right],$$

where T is temperature and V is volume of molecular system.

The computation of the individual terms of the partition function and their derivatives, except of the configurational integral, is dealt with in the works of Lucas. [7]

The various derivatives and expressions of the fundamental equations (2.3) have an important physical significance. This paper presents expressions that are very important for designing the energy-conversion processes. The various derivatives also prove to be of physical interest:

$$\text{Coefficient of thermal expansion: } \beta = \frac{1}{V} \left(\frac{\partial V}{\partial T} \right)_p. \quad (2.4)$$

$$\text{Isothermal compressibility: } \chi = -\frac{1}{V} \left(\frac{\partial V}{\partial p} \right)_T. \quad (2.5)$$

$$\text{Molar heat capacity at constant volume: } C_v = \left(\frac{\partial U}{\partial T} \right)_V. \quad (2.6)$$

$$\text{Molar heat capacity at constant pressure: } C_p = \left(\frac{\partial H}{\partial T} \right)_p = C_v + \frac{TV\beta^2}{\chi}. \quad (2.7)$$

$$\text{Speed of sound: } c_0 = \sqrt{-V^2 \frac{1}{M} \left(\frac{\partial p}{\partial V} \right)_s} = \sqrt{-V^2 \frac{\frac{C_p}{T} \left(\frac{\partial T}{\partial V} \right)_p \frac{1}{M}}{\left(\frac{\partial V}{\partial T} \right)_p - \frac{C_p}{T} \left(\frac{\partial T}{\partial p} \right)_v}}, \quad (2.8)$$

where M is molar mass.

$$\text{The Joule-Thomson coefficient: } \mu_J = \frac{1}{C_p} \left[T \left(\frac{\partial V}{\partial T} \right)_p - V \right]$$

3 SECOND VIRIAL COEFFICIENT AND HIGHER ORDERS OF VIRIAL COEFFICIENTS

Calculation of second virial coefficient for real substances is possible with both classical and statistical thermodynamics. Classical thermodynamics has no insight into the microstructure of the substance, but it allows the calculation of the thermodynamic function of state with the assistance of measurement or empirical equations. Statistical thermodynamics, in contrast, calculates the properties of state on the basis of molecular motions in a space, and on the basis of the intermolecular interactions.

The virial equation of state is the expansion of the compressibility factor Z_r along individual isotherms in terms of density, according to the next equation:

$$Z_r = \frac{pV}{NkT} = 1 + \frac{B_2}{V} + \frac{B_3}{V^2} \dots\dots\dots \quad (3.1)$$

where B_2 and B_3 are second and third virial coefficient and are defined as:

$$B_2 = \left(\frac{\partial Z_r}{\partial n} \right)_{n=0} = \left(\frac{\partial Z_r}{\partial \rho} \right)_{\rho=0},$$

$$B_3 = \frac{1}{2!} \left(\frac{\partial^2 Z_r}{\partial n^2} \right)_{n=0} = \frac{1}{2!} \left(\frac{\partial^2 Z_r}{\partial \rho^2} \right)_{\rho=0} \quad (3.2)$$

The virial coefficients are properties of the gas at $n=0$. The second virial coefficient is the first term of the expansion of the compressibility factor of a fluid in powers of the density. From statistical mechanics, the second virial coefficient summarizes the influence of two body interactions; the third virial coefficient summarizes influences of three-body interactions, and so on. They are properties of gas at $n=0$ and they do not depend on density, but only on temperature and (in mixtures) on composition. A general expression for virial coefficients related with the equation of state can be written with the next equation:

$$B_k = \frac{1}{(k-1)!} \left(\frac{\partial^{k-1} Z_r}{\partial \rho^{k-1}} \right)_{\rho=0} \quad (3.3)$$

In this paper, we have used the combination of equations (3.2) and the method of statistical mechanics. On this basis, we can express the free energy of a fluid as the sum of all parts:

$$A = A^{LJ} + A^{ex} \quad (3.4)$$

On the basis of Eq. (3.4), we can express

$$B = B_{LJ} + B_{ex} \quad (3.5)$$

If the virial coefficients are known as a function of temperature, all thermodynamic functions depending on the equation of state may be calculated:

$$U_{conf} = -NkT^2 \left[n \frac{dB_2}{dT} + \frac{n^2}{2} \frac{dB_3}{dT} + \dots\dots\dots \right] \quad (3.6)$$

$$S_{conf} = -Nk \left[\left(B_2 + T \frac{dB_2}{dT} \right) n + \left(B_3 + T \frac{dB_3}{dT} \right) \frac{n^2}{2} + \dots\dots\dots \right] \quad (3.7)$$

4 STATISTICAL THERMODYNAMICS

A. Revised Cotterman model (CYJ)¹¹

A revised Cotterman EOS is based on the hard sphere perturbation theory. The average relative deviation for pressure and internal energy in comparison with Monte-Carlo simulations are 2.17% and 2.62%, respectively, for 368 data points.[9] The configurational free energy is given by:

$$A_{LJ} = A_{hs} + A_{pert} \quad (4.1)$$

$$\frac{A_{hs}}{R_m T} = \frac{4\eta - 3\eta^2}{(1 - \eta)^2}, \quad (4.2)$$

$$A_{pert} = \frac{A^{(1)}}{T^*} + \frac{A^{(2)}}{T^{*2}} \quad (4.3)$$

$$\frac{A^{(1)}}{R_m T} = \sum_{m=1}^4 A_{1m} \left(\frac{\eta}{\tau}\right)^m, \quad \frac{A^{(2)}}{R_m T} = \sum_{m=1}^4 A_{2m} \left(\frac{\eta}{\tau}\right)^m, \quad (4.4)$$

$$\tau = 0.7405, \quad \eta = \frac{\pi \rho d^3}{6}, \quad (4.5)$$

where η is packing factor, D is hard-sphere diameter. The effective hard sphere diameter d is determined on the basis of Barker perturbation theory. We use a function developed in the work of Chapman et al. [9]

$$d = \sigma \frac{1 + 0.2977T^*}{1 + 0.33163T^* + 0.0010477T^{*2}} \quad (4.6)$$

With the help of configurational free energy, we can calculate all configurational thermodynamic properties. Expressions for the calculation of configurational entropy and internal energy are shown in literature.[9] We carried out all other expressions for the calculation of thermo-physical properties.

B. Determination of virial coefficients for LJ model

In the broadest sense, we can express the n -th virial coefficient as the sum of two parts:

$$B_{nLJ} = B_{nhs} + B_{npert} \quad (4.7)$$

The first part in Equation (4.7) represents hard sphere part, while the second part represents the perturbation theorem where the effects of polarity are also hidden. On the basis of Equation (3.2), we made the next analytical expressions:

$$B_{2hs} = \frac{2\pi d^3}{3}, \quad B_{3hs} = 10 \left(\frac{\pi d^3}{6}\right)^2, \quad B_{4hs} = 18.3648 \left(\frac{\pi d^3}{6}\right)^3, \quad (4.8)$$

$$B_{5hs} = 28.2245 \left(\frac{\pi d^3}{6} \right)^4, \quad B_{6hs} = 39.83 \left(\frac{\pi d^3}{6} \right)^5,$$

$$B_{2pert} = \frac{d^3}{\sqrt{2}} \left(\frac{A_{11}}{T^*} + \frac{A_{21}}{T^{*2}} \right), \quad B_{3pert} = d^6 \left(\frac{A_{12}}{T^*} + \frac{A_{22}}{T^{*2}} \right), \quad (4.9)$$

$$B_{4pert} = \frac{3d^9}{2^{1.5}} \left(\frac{A_{13}}{T^*} + \frac{A_{23}}{T^{*2}} \right), \quad B_{5pert} = d^{12} \left(\frac{A_{14}}{T^*} + \frac{A_{24}}{T^{*2}} \right), \quad B_{6pert} = 0 \quad (4.10)$$

A. Intermolecular potential

Attractive intermolecular potential consists in general of three parts:

a. Multipole or electrostatic force potential, which occurs due to the manifestation of static permanent dipole, quadrupole and multipole moments or asymmetrical distribution of the charge in molecules. In this case, the summation of Coulomb's interactions between positive charged nuclei and negative charged electrons of a certain molecule with the adequate charges of another molecule gives (in general) a certain value of intermolecular energy. The interactions between molecules possessing multipole moments result in attractive forces, which are dependent on the orientation of molecules in space. The distribution of charges can (in general) be described or denoted by multipole molecule moments. Fig. 1 illustrates some of the lowest rates. A neutral atom with the negative cloud centre of gravity coinciding with the centre of gravity of positive nucleus has a zero dipole moment. The first rate of multipole moments is called the **dipole moment** and is created if the centres of gravity of positive and negative charges fail to coincide. It is represented by a partial positive and negative moment δ at a certain distance r , which creates the moment $r\delta$. In many cases, the molecules have no dipole moments due to the symmetry of charges. Nevertheless, they can have even higher rates of multipole moments, e.g. quadrupole and octopole moments.

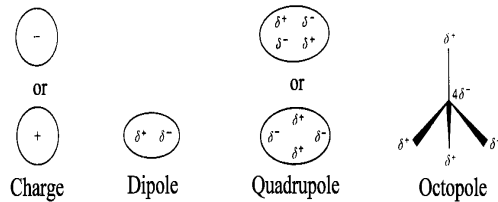


Figure 1: Molecular multipole moments

In general, multipole moments can be written as tensors in the Cartesian coordinate system³:

$$\text{Molecule charge: } q = \int \rho \cdot d\vec{r}$$

$$\text{Dipole: } \mu_\alpha = \int \rho \alpha \cdot d\vec{r}$$

$$\text{Quadrupole: } \theta_{\alpha\beta} = \frac{1}{2} \int \rho (3\alpha\beta - r^2 \delta_{\alpha\beta}) d\vec{r} \quad (4.11)$$

$$\text{Octopole: } \Omega_{\alpha\beta\gamma} = \frac{1}{2} \int \rho [5\alpha\beta\gamma - r^2 (\alpha\delta_{\beta\gamma} + \beta\delta_{\gamma\alpha} + \gamma\delta_{\alpha\beta})] d\vec{r}$$

$$\delta_{\alpha\beta} = 1, \text{ if } \alpha = \beta; \delta_{\alpha\beta} = 0, \text{ if } \alpha \neq \beta.$$

Higher rates may be defined as well, but they are rarely used in calculations.

b. Induction force potential. The neutral atom with the negative electron cloud centre of gravity coinciding with the centre of gravity of the positive nucleus has no dipole moment. If, for example, such an atom is approached by another atom with a dipole moment, the dipole moment $\vec{\mu}_{\text{ind}}$ is induced in it, proportional to the electric field of the dipole moment \vec{E} :

$$\vec{\mu}_{\text{ind}} = \alpha \vec{E}. \quad (4.12)$$

The described phenomenon is called polarization. The constant α is called the polarization constant. The polarization effect occurs also when two molecules with multipole moments approach one another (Figure 2).

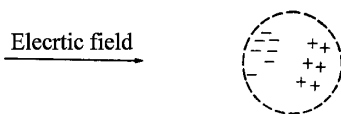


Figure 2: Molecule polarization

In general, the polarization constant in the system of molecules with multipole moments is a tensor. [3] The analytical calculation of tensor components of the polarization constant is very complex. In practical computations, we usually satisfy ourselves by the mean polarization constant:

$$\alpha = \frac{1}{3} (\alpha_{xx} + \alpha_{yy} + \alpha_{zz}). \quad (4.13)$$

The electrostatic and inductive potentials occur in the case of polar molecules, where the potential energy is not dependent on the distance only, but on the influence of the orientation of molecule in space.

c. Dispersion force potential occurs both in polar and nonpolar molecules. It results from time-varying dipole moments. In most cases, the potential of dispersion forces represents the most important element. In general, an example of nonpolar molecules can be expressed by the following relation:

$$u_{\text{disp}} = \frac{C_1}{r^6} + \frac{C_2}{r^8} + \frac{C_3}{r^9} \quad (4.14)$$

The total intermolecular potential can be written as a sum of the Lennard-Jones's intermolecular potential (LJ) and the potential that also takes into account the orientation of a molecule in space (p):

$$u_{12}(r_{12}, \omega_1, \omega_2) = u_{12}^{\text{LJ}}(r_{12}) + u_{12}^{\text{p}}(r_{12}, \omega_1, \omega_2) \quad (4.15)$$

In Equation (2.6), r_{12} is the distance of centres of gravity between the molecules 1 and 2, ω_1 and ω_2 are orientations of both molecules in space, which may be expressed with Euler's angles (ϕ , ϑ , χ). The reference part u^{LJ} can be written also as a certain mean intermolecular energy at the distance r_{12} :

$$u_{12}^{\text{LJ}}(r_{12}) = \langle u_{12}(r_{12}, \omega_1, \omega_2) \rangle_{\omega_1 \omega_2} = \frac{\int u_{12}(r_{12}, \omega_1, \omega_2) d\omega_1 d\omega_2}{\int d\omega_1 d\omega_2} \quad (4.16)$$

Now suppose that the sum of intermolecular potential energy is:

$$U_{\text{conf}} = \sum_{i < j} u_{ij} = \sum_{i < j} u_{ij}^{\text{LJ}}(r_{ij}) + \sum_{i < j} u_{ij}^{\text{p}}(r_{ij}, \omega_i, \omega_j) \quad (4.17)$$

Using the perturbation expansion around the reference potential, one can then write the configuration effect to the free energy as:

$$\frac{A_{\text{conf}}}{Nk_{\text{B}}T} = \frac{A^{\text{LJ}}}{Nk_{\text{B}}T} + \frac{A^{\lambda}}{Nk_{\text{B}}T} + \frac{A^{\lambda\lambda}}{Nk_{\text{B}}T} + \frac{A^{\lambda\lambda\lambda}}{Nk_{\text{B}}T} \quad (4.18)$$

There are several methods for computing the influence of anisotropic potentials [5–12]. In this paper, those models that yielded favourable results in practical computations for a large number of components and within a relatively wide range of densities and temperatures were used.

The perturbation theory is applied successfully to real fluids of moderate polarity and to molecules with a simple structure. The problem in perturbation theory is that in the series of the perturbation, expansion converges slowly as the dipole moment increases. The application of the Pade equation can help the equation converge more rapidly. However, if a simple reference model is used for highly polar molecules, the perturbation terms become greater than the reference term, which in principle is not a small perturbation on which the theory of small perturbation is based. From scientific point of view, it is impossible to calculate the thermodynamic properties for highly polar molecules on the basis of perturbation theory. In this paper, we have used the mean potential model, instead of the statistical-mechanical perturbation theory, to avoid the aforementioned problems. The orientation-averaged pair potential for polar molecules is given by the next equations:

$$u^{\text{ave}} = 4\varepsilon' \left[\left(\frac{\sigma'}{r} \right)^{12} - \left(\frac{\sigma'}{r} \right)^6 \right] \quad (4.19)$$

where:

$$\varepsilon' = \varepsilon \left(1 + \frac{\mu^4}{6kT\varepsilon\sigma^6} + \dots \right) \quad (4.20)$$

and

$$(\sigma')^6 = \frac{\sigma^6}{\left(1 + \frac{\mu^4}{12kT\varepsilon\sigma^6} + \dots \right)} \quad (4.21)$$

In the presented equation, the most important term in the multipole expansion, the dipole-dipole interaction, is taken into account.

5 RESULTS AND DISCUSSION

In this paper, we have shown the analytical computations for virial coefficients for ethane and carbon dioxide. Figures 3 and 4 show the analytical calculation of second, third and higher orders of virial coefficients for ethane and carbon dioxide in comparison with the REFPROP 7.1 program. [13] The REFPROP program is one of the most accurate programs for calculating thermodynamic and transport properties in fluids.

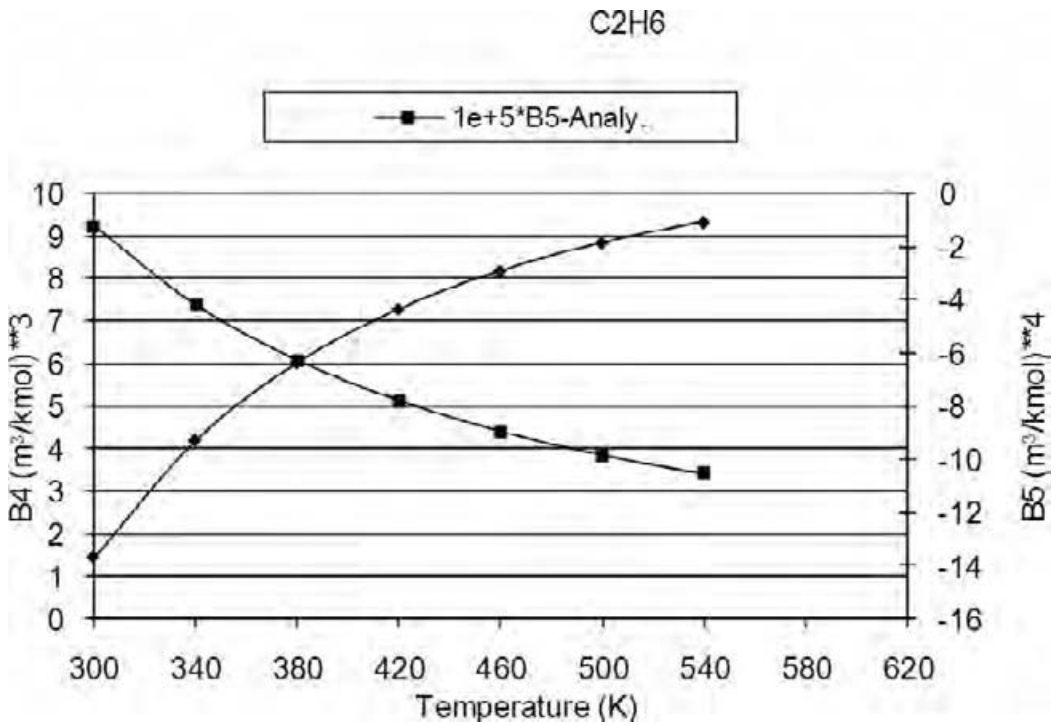
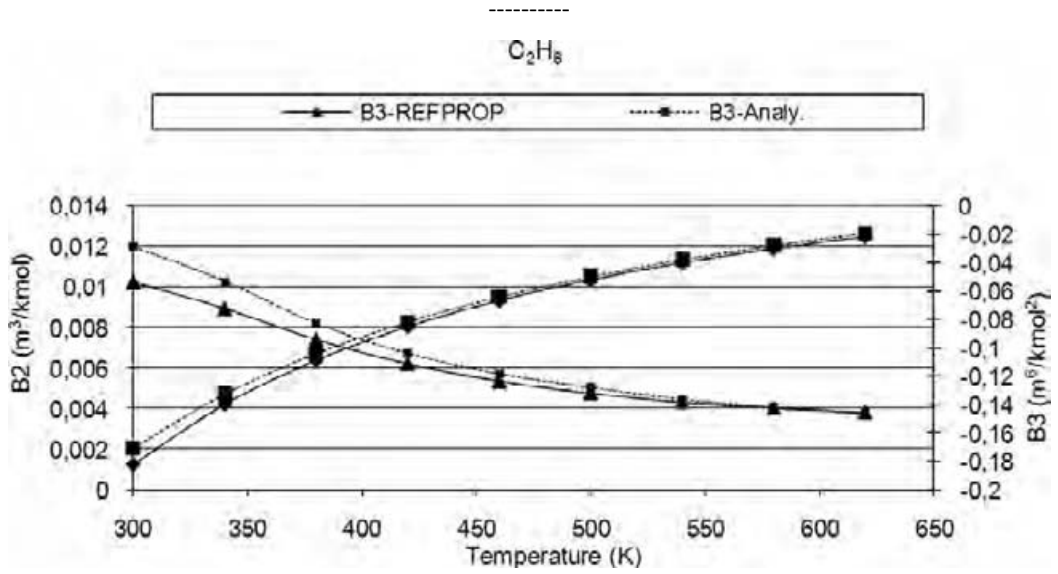


Figure 3: Virial coefficients for ethane

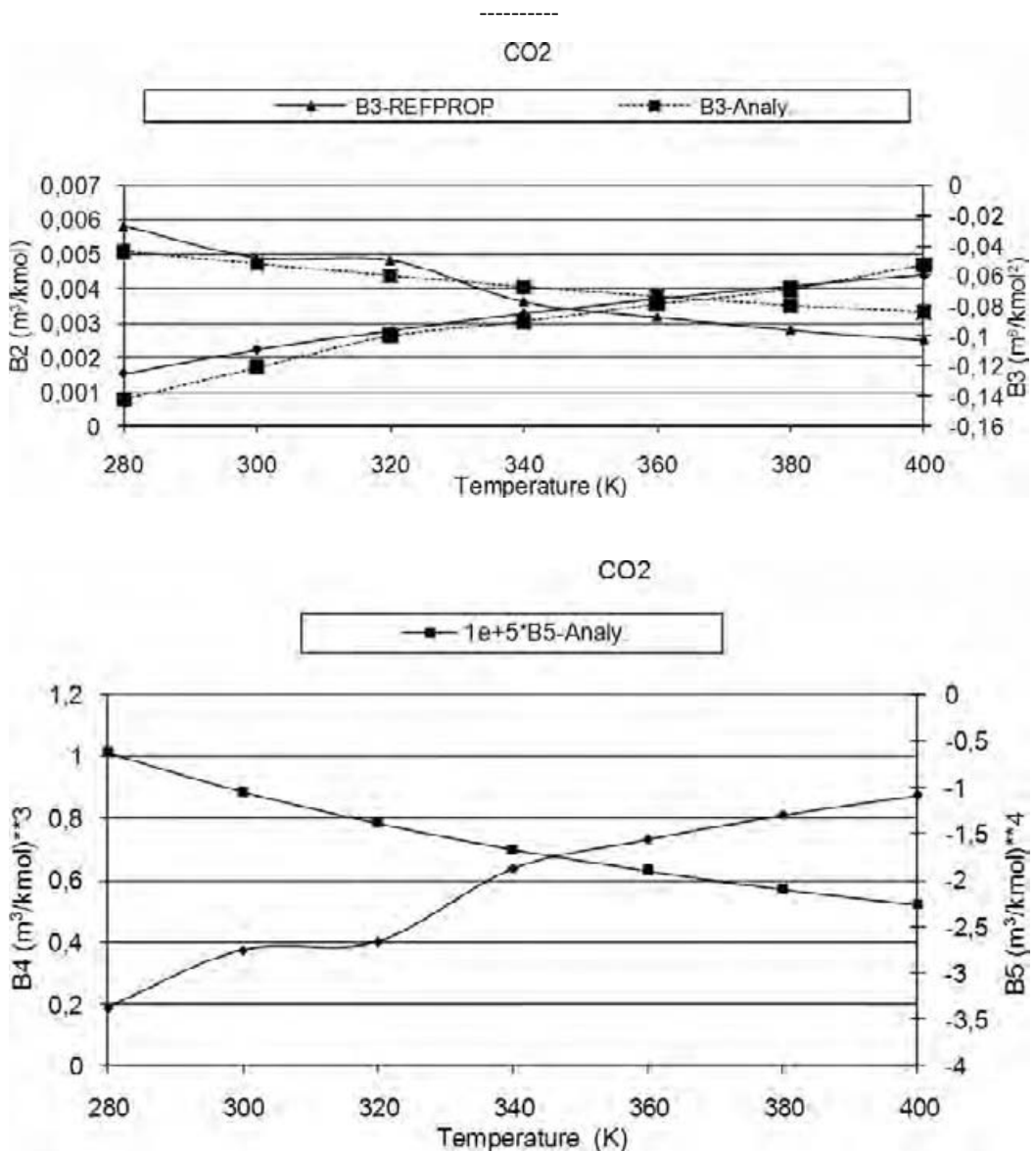


Figure 4: Virial coefficients for carbon dioxide

References

- [1] Kumar, S., Khanna, K.N. "Virial Coefficients from Equation of State", Journal of Molecular Liquids, Vol. 107, No. 1-3, 2003, pp. 41–57.
- [2] Boublik, T., Nezbeda, I., "P-V-T Behaviour of Hard Body Fluids, Theory and Experiment", Collection Czechoslovak Chem. Commun., Vol. 51, 1986, pp. 2301–2433.
- [3] Jenaček, J., Boublik, T., "The second virial coefficient of polar-rod-like Molecules", Fluid Phase Equilibria, Vol. 212, 2003, pp.: 349–361.

-
- [4] **Walas, S.M.**, *Phase Equilibria in Chemical Engineering*, 1984, Buittenworth Publishers, Boston.
- [5] **Avsec, J.**, "Calculation of Transport Coefficients of R-32 and R-125 with the methods of Statistical Thermodynamics and Kinetic Theories of Gas", *Archives of Thermodynamics*, Vol. 24, No. 3, pp. 69–82.
- [6] **Avsec J., Di Nicola, G. Marčič, M., Polonara, F.**. *Second virial coefficient for pure HFC refrigerants and their mixtures + R744 - theoretical calculations in comparison with experimental data*. V: Fifteenth symposium on thermophysical properties, Boulder, Colorado USA, June 22-27, 2003. Boulder: National Institute of Standards and Technology, 2003, 18ff.
- [7] **Lucas, K.**, *Applied Statistical Thermodynamics*, Springer - Verlag, 1992, New York.
- [8] **Gray, C.G., Gubbins, K.E.**, *Theory of Molecular Fluids*, Clarendon Press, 1984, Oxford.
- [9] **Avsec J., Marcic, M., Watanabe, K.**, "Study for Lennard-Jones Chains for Hydrocarbons", *J. thermophys. heat transf.*, vol. 18, no. 2, 2004, pp. 243–252.
- [10] **Avsec, J., Marčič, M.** "Influence of Multipolar and Induction Interactions on the Speed of Sound". *J. thermophys. heat transf.*, 2000, vol. 14, no. 4, str. 496–503.
- [11] **Chung, T.H., Khan, M.M., Lee, L.L., Starling, K.E.**, "A New Equation of State for Polar and Nonpolar Pure Fluids", *Fluid Phase Equilibria*, Vol. 17, 1984, pp.: 351–372
- [12] **Chunxi, L., Yigui, L., Jiufang, L.** "Investigation and Improvement of Equations of State for Lennard-Jones Fluid", *Fluid Phase Equilibria*, Vol. 127, 1997, pp. 71–81.
- [13] **Lemmon, E.W., Jacobsen, R.T.**, "A Generalized Model for the Thermodynamic Properties of Mixtures", *International Journal of Thermophysics*, Vol. 20, No. 3, 1999, pp.825–834.

Nomenclature

(Symbols)	(Symbol meaning)
A	free energy
B₂, B₃, B₄	second, third, fourth virial coefficient
c₀	velocity of sound
C_p	molar heat capacity at constant pressure
C_v	molar heat capacity at constant volume
D	hard sphere diameter
f	number of degrees of freedom
G	free enthalpy

g_0	hard sphere radial distribution function
H	enthalpy
k	Boltzmann constant
M	molecular mass
N	number of molecules in system
p_p	pressure, momentum
R_m	universal gas constant
S	entropy
T	temperature
T^*	reduced temperature
U	internal energy
v	specific volume
V	volume
Z	partition function

EXPERIMENTAL AND NUMERICAL ANALYSIS OF THE IMPACT OF PARTICLES ON THE DEVELOPMENT OF CAVITATION FLOW AROUND A HYDROFOIL

EKSPERIMENTALNA IN NUMERIČNA ANALIZA VPLIVA DELCEV NA RAZVOJ KAVITACIJE OKOLI LOPATIČNEGA PROFILA

Boštjan Gregorc[✉], Matjaž Hriberšek, Andrej Predin

Keywords: cavitation flow; particle; experiment; numerical simulations

Abstract

The purpose of this paper is to present an analysis of the impact of solid particles on the development of cavitation flow conditions around a NACA hydrofoil. Experimental studies have been conducted in a cavitation tunnel with different mixtures of sand and water. Experimental measurements of torque versus hydrofoil with different mixtures have been performed. To model the liquid-vapour phase change, a simplified Rayleigh-Plesset equation was used. The effect of particles on the development of cavitation flows was modeled using an additional phase particle dispersion model (Euler-Euler). For numerical modelling, the CFX 12.1 software package was used. This paper presents the results of experimental measurements and their comparison with numerical simulations.

Povzetek

Namen tega prispevka je predstaviti analizo učinkov trdnih delcev na kavitacijske tokovne razmere okoli lopatičnega profila NACA. Eksperimentalne študije so bile izvedene v kavitacijskem tunelu z različnimi mešanici mulja in vode. Opravljeno je bilo eksperimentalno

[✉] Corresponding author: Boštjan Gregorc, Tel.: +386 (0)2 300 5295, Fax: +386 (0)2 300 5691, E-mail address: bostjan.gregorc@dem.si

merjenje navora na lopatični profil. Pri modeliranju fazne spremembe je bila uporabljena poenostavljena Rayleigh-Plessetova enačba. Za modeliranje vpliva delcev na razvoj kavitacijskih tokov je bil uporabljen model dodatne disperzije delcev (Euler-Euler model). Za numerično modeliranje je bil uporabljen programski paket CFX 12,1. V prispevku so predstavljeni rezultati eksperimentalnih meritev in njihova primerjava z numeričnimi simulacijami.

1 INTRODUCTION

A large amount of hydraulic machinery working in silt-laden rivers encounters serious problems of silt abrasion and aggravated cavitation. In simple cases, machine performance is impaired, while structural damage may result in serious cases. Recently, many hydraulic engineers are encountering serious challenges in solving the problems of silt-laden flow in many hydro projects. The effect of particles (sand) on the development of cavitation and hydrodynamic forces impacts the performance of a hydraulic machine.

Cavitation is closely associated with local end-time variable properties, such as local velocity and thermodynamic pressure, which is lower than the vapourising pressure of the liquid at an operating temperature of the system. The authors of the experimental studies discovered a number of instabilities, among which the pulse cavitation cloud [1,3] is the most pronounced. Research areas in recent decades are based on the mutual interaction between the liquid and the vapour phases. There are also many research papers [2,11] on the impact of undissolved air, impurities and particles in the development of cavitation flow, and consequently well-developed erosion and increased abrasion in the turbine and pump parts. Z.Y. Mei and Y.L. Wu [8,19] established that cavitation in water, due to the presence of particles (sand), occurs earlier than in the case of pure water. Particles affect the relative cavitation length of the vapour phase, as well as cavitation fluctuation. Mass concentrations of particles, in which the largest increase of the vapour phase occurs, are between 8 and 13 kg/m³ [2]. For the mass concentration ξ_c , less than 8–13 kg/m³, the particle plays a role of inducing cavitation, whereas for ξ_c greater than 8–13 kg/m³ it has a retarding effect.

Determining the development of the vapour phase with numerical simulation is a faster and cheaper development of improved hydraulic shapes. Research papers of the effects on turbulent cavitation flow are mostly based on the Navier-Stokes equations [4,7,15,20]. An example of the cavitation flow modeling results from the multiphase flow, where they were developed on the basis of two-liquid model (Euler-Euler). Cavitation two-phase flow is calculated based on two continuing phases (liquid and vapour) as a composition of two phases. In the case of only one phase, the cavitation flow can be written (vapourisation-condensation) as cavitation model, according to A.K. Singhal [12]. Given the use of different models to simulate the cavitation flow, each phase can be described by different combinations (mixtures) [13]. The influence of impurities, undissolved gases and particles in models to describe the phase flow is usually not covered. For interaction particles, vapour phase and water, the use of mass continuity equation and momentum equation is necessary. Authors often use the mixture and particle model to integrate undissolved gas mixture in the cavitation flow. A.K. Singhal [21] has used the mass fraction equation and the k- ϵ turbulence model to simulate the cavitating flow around a hydrofoil. W. H. Brewer and S. A. Kinnas [17] used a multiple species approach with additional establishment of a mass transfer law between liquid and vapour. This model can be applied even when the relative motion between phases should be taken into count. M. Mikko et al. [13] note the applicability of mixture model for multiphase flow in their study. T.

Aschenbrenner et al. [15] used the mixture model and full cavitation model [12] to compute the unsteady turbulent flow and compared it with experiment. From the vapourisation and condensation mechanics between vapour-liquid and the assumption of unchanged pressure in vapour, the mass change rate of vapour is proportional to liquid pressure and vapour pressure difference.

2 GOVERNING EQUATIONS AND NUMERICAL ADJUSTMENTS

2.1 Inhomogeneous model-multiphase flow

The equations that describe the development of cavitation can appear as a two- or three-phase system. Most frequently, the Navier-Stokes equations of viscous flow and conventional k-ε turbulence model are used. This article describes the situation between the continuous phase (water) and vapour and takes into account the proportion of solid particles throughout the suspension (in total suspension). The three components of the flow are:

- liquid (continuous phase),
- vapour (continuous phase),
- particle (dispersed solid).

The Euler-Euler formulation is based on the assumption of interpenetrating continua [4,13]. A separate set of mass and momentum conservation equations is solved for each phase. Interphase transfer terms must be modeled to account for the interaction of the phases.

The record of each volume fraction can be written:

$$\alpha_l + \alpha_v + \alpha_d = 1 \quad (2.1)$$

where α - stands for the volume fraction, d for dispersed solid, l for liquid, and v for vapour in the primary phase. The volume fraction of vapour phase and water varies in dependence of the developed vapour phase. The average proportion of solid particles does not change in volume (an input), while the local fraction of particles varies due to developed vapour phase. The mixture density ρ_m can be written with volume fraction:

$$\rho_m = \rho_l(1 - \alpha_d - \alpha_v) + \alpha_d \rho_d + \alpha_v \rho_v \quad (2.2)$$

Determination of mixture viscosity can be written:

$$\mu_m = \mu_l(1 - \alpha_d - \alpha_v) + \alpha_d \mu_d + \alpha_v \mu_v \quad (2.3)$$

The impact of particles on the development of cavitation is observed with the dispersion flow. The governing equations of vapour-liquid-dispersion phase flow are as follows;

Continuity equation of water, vapour and particles:

$$\frac{\partial(\alpha_l \rho_l)}{\partial t} + \nabla(\alpha_l \rho_l v_l) = \sum_{v=1}^{N_p} \Gamma_{lv} \quad (2.4)$$

$$\frac{\partial(\alpha_v \rho_v)}{\partial t} + \nabla(\alpha_v \rho_v v_v) = \sum_{l=1}^{N_p} \Gamma_{vl} \quad (2.5)$$

$$\frac{\partial(\alpha_d \rho_d)}{\partial t} + \nabla(\alpha_d \rho_d v_d) = 0 \quad (2.6)$$

Γ_{lv} - the mass flow rate per unit volume from liquid phase to vapour phase.

Momentum equations of liquid (water), vapour and particles:

$$\frac{\partial(\alpha_l \rho_l v_l)}{\partial t} + \nabla \left(\alpha_l (\rho_l v_l \cdot v_l) \right) = -\alpha_l \nabla p_l + \nabla \left(\alpha_l \mu_l (\nabla v_l + (\nabla v_l)^T) \right) + \sum_{v=1}^{N_p} (\Gamma_{lv} v_v - \Gamma_{vl} v_l) + F_{il} \quad (2.7)$$

$$\frac{\partial(\alpha_v \rho_v v_v)}{\partial t} + \nabla \left(\alpha_v (\rho_v v_v \cdot v_v) \right) = -\alpha_v \nabla p_v + \nabla \left(\alpha_v \mu_v (\nabla v_v + (\nabla v_v)^T) \right) + \sum_{l=1}^{N_p} (\Gamma_{vl} v_l - \Gamma_{lv} v_v) + F_{iv} \quad (2.8)$$

$$\frac{\partial(\alpha_d \rho_d v_d)}{\partial t} + \nabla \left(\alpha_d (\rho_d v_d \cdot v_d) \right) = -\alpha_d \nabla p_d + \nabla \left(\alpha_d \mu_d (\nabla v_d + (\nabla v_d)^T) \right) + F_{id} \quad (2.9)$$

F_i – the interfacial forces (drag and solid particle collision models) acting on phase (l, v, d) due to the presence of other phases ($F_{il} = D_{drag,ld} + F_{cm,ld}$), $(\Gamma_{lv} v_v - \Gamma_{vl} v_l)$ – represents momentum transfer induced by interphase mass transfer (vapour and liquid).

For mass transfer processes across a phase interphase, it is useful to express the volumetric mass sources in terms of mass fluxes:

$$\Gamma_{lv} = \dot{m}_{lv} A_{lv} \quad (2.10)$$

\dot{m}_{lv} is the mass flow rate per unit interfacial area from liquid phase to vapour phase (cavitation model), and is the interfacial area density between the phases; A_{lv} is the interfacial area density between the phases (liquid, vapour).

2.2 Solids Stress Tensor

Additional stresses due to inter-particle collisions are modeled using a collisional solids stress tensor in the solid phase momentum equation only:

$$\tau_{dij} = -p_d \delta_{ij} + \mu_d \left(\frac{\partial v_i}{\partial x_j} + \frac{\partial v_j}{\partial x_i} + \frac{2}{3} \frac{\partial v_k}{\partial x_k} \delta_{ij} \right) \quad (2.11)$$

p_d is solids pressure, μ_d is solids shear viscosity. Interfacial transfer of momentum and mass is directly dependent on the contact surface area between the two phases. Interfacial transfer can be modeled using either the particle or mixture models. These essentially provide different algebraic prescriptions for the interfacial area density.

2.3 Particle model

The Particle model is used for the interfacial transfer of momentum between two phases (water particles and vapour particles). The surface area per unit volume is then calculated by assuming that phase (particles) is present as spherical particles of Mean Diameter - d_d . Using this model, the interphase contact area is:

$$A_{ld} = \frac{6\tilde{\alpha}_d}{d_d} \quad (2.12)$$

$$\tilde{\alpha}_d = \left\{ \begin{array}{ll} \max(\alpha_d, \alpha_{\min}) & \text{if } (\alpha_d < \alpha_{\min}) \\ \max\left(\frac{1-\alpha_d}{1-\alpha_{\max}} \alpha_{\max}, \alpha_{\min}\right) & \text{if } (\alpha_d > \alpha_{\min}) \end{array} \right\} \quad (2.13)$$

$$D_{\text{drag,ld}} = A_{\text{ld}} \rho_l \frac{C_D}{8} |v_d - v_l| \quad (2.14)$$

This model is modified for robustness purposes in two ways: α_d is clipped to a minimum volume fraction to ensure the area density does not go exactly to zero and for large α_d , (i.e. when the dispersed phase assumption of being dispersed is invalid) the area density is decreased to reflect the fact that it should lead to zero α_d as tends to 1 [4].

2.4 Mixture model

This model is used for the interfacial transfer of momentum between the water phase and the vapour phase [4,13]. The surface area per unit volume is calculated from:

$$A_{\text{lv}} = \frac{6\alpha_l\alpha_v}{\alpha_l l_v + \alpha_v l_l} \Rightarrow l_{\text{lv}} = \frac{\alpha_l l_v + \alpha_v l_l}{6} \quad (2.15)$$

$$\rho_{\text{lv}} = \alpha_l \rho_l + \alpha_v \rho_v \quad (2.16)$$

$$D_{\text{drag,lv}} = C_D \rho_{\text{lv}} A_{\text{lv}} |v_v - v_l| (v_v - v_l) \quad (2.17)$$

l_i - interfacial length scale, F_{lv} - total drag exerted by vapour phase on liquid phase per unit volume.

2.5 Rayleigh-Plesset Model

The Rayleigh-Plesset model is implemented in the multiphase framework as an interphase mass transfer model in the numerical code used. The Rayleigh-Plesset equation provides the basis for the rate equation describing the growth of a gas bubble in a liquid and is given by:

$$R_B = \frac{d^2 R_B}{dt^2} + \frac{3}{2} \left(\frac{R_B}{dt} \right)^2 + \frac{2\sigma_s}{\rho_l R_B} = \frac{p_v - p}{\rho_l} \quad (2.18)$$

in which R_B represents the bubble radius, p_v is the pressure in the bubble (assumed to be the vapour pressure at the liquid temperature), p is the pressure in the liquid surrounding the bubble, ρ_l is the liquid density, and σ_s is the surface tension coefficient between the liquid and vapour. If we neglect the second order terms (which is appropriate for low oscillation frequencies) and the surface tension, this equation reduces to:

$$\frac{dR_B}{dt} = \sqrt{\frac{2}{3} \frac{p_v - p}{\rho_l}} \quad (2.19)$$

The rate of change of bubble volume follows as:

$$\frac{dV_B}{dt} = \frac{d}{dt} \left(\frac{2}{3} \pi v R_B^3 \right) = 4\pi R_B^2 \sqrt{\frac{2}{3} \frac{p_v - p}{\rho_l}} \quad (2.20)$$

And the rate of change of bubble mass is:

$$\frac{dm_B}{dt} = \frac{dV_B}{dt} \rho_v = 4\pi R_B^2 \rho_v \sqrt{\frac{2}{3} \frac{p_v - p}{\rho_l}} \quad (2.21)$$

Let N_B be bubbles per unit volume. Then the volume fraction r_v can be expressed as:

$$r_v = N_B V_B = \frac{4}{3} \pi R_B^3 N_B \quad (2.22)$$

Total interphase mass transfer rate per unit volume is:

$$\dot{m}_{lv} = \frac{3r_v \rho_v}{R_B} \sqrt{\frac{2}{3} \frac{p_v - p}{\rho_l}} \quad (2.23)$$

This equation can be written after the implementation of:

$$\dot{m}_{lv} = F \frac{3r_{nuc}(1-r_v)\rho_v}{R_{nuc}} \sqrt{\frac{2}{3} \frac{|p_v - p|}{\rho_l}} \operatorname{sgn}(p_v - p) \quad (2.24)$$

where F is an empirical factor which may differ for condensation and vapourization, r_{nuc} is the volume fraction of the nucleation sites (case of condensation), designed to account for the fact that they may occur at different rates (condensation is usually much slower than vapourization). For modelling purposes, the bubble radius R_B will be replaced by the nucleation site radius R_{nuc} . Despite the fact that the previous equations have been generalized for vapourization and condensation, it requires further modification in the case of vapourization [4]. Vapourization is initiated at nucleation sites (most commonly non-condensable gases). As the vapour volume fraction increases, the nucleation site density must decrease accordingly, since there is less liquid. For vapourization, r_v is replaced by $r_{nuc}(1 - r_v)$. The Rayleigh-Plesset cavitation model implemented in CFX uses the following defaults for the model parameters: $R_{nuc} = 1 \mu\text{m}$, $r_{nuc} = 5E - 4$, $F_{cond} = 0.01$ ($p_v - p < 0$), $F_{vap} = 50$ ($p_v - p > 0$) [7].

Calculation of the cavitating flow is limited by a variety of empirical data that are often useful only for a given area and do not apply in general terms.

2.6 Turbulence model

When solving the turbulent flow of the cavitating liquid multi-phase flow, the Reynolds averaged Navier-Stokes solver (RANS) is used in the present work. The turbulence model is necessary in it. O. Coutier-Delgosha et al. [14] evaluated the turbulence model influence on the numerical simulations of unsteady cavitation flow:

$$\frac{\partial k}{\partial t} + \tilde{v}_j \frac{\partial k}{\partial x_j} = \frac{\partial}{\partial x_i} \left[\left(\mu_i + \frac{\partial \mu_T}{\partial \sigma_k} \right) \frac{\partial k}{\partial x_i} \right] + P - \varepsilon, \quad (2.25)$$

$$\frac{\partial \varepsilon}{\partial t} + \tilde{v}_j \frac{\partial \varepsilon}{\partial x_j} = \frac{\partial}{\partial x_i} \left[\left(\mu_i + \frac{\partial \mu_T}{\partial \sigma_\varepsilon} \right) \frac{\partial \varepsilon}{\partial x_i} \right] + C_{1\varepsilon} \frac{\varepsilon}{k} P - C_{2\varepsilon} \frac{\varepsilon^2}{k}, \quad (2.26)$$

in which the standard values of the constants are [19]: $C_\mu = 0.09$, $\sigma_k = 1.0$, $\sigma_\varepsilon = 1.3$, $C_{1\varepsilon} = 1.44$, $C_{2\varepsilon} = 1.92$

Using the RNG k-ε turbulence model, we obtain (according to results) a minor impact on the vapour phase to torque blade, as well as compared to the developed form of a cloud. For this reason, we considered compressibility flow or change of turbulent viscosity and effects on kinetic energy.

$$\mu_t = f(\rho_{IV}) C_\mu \frac{k^2}{\epsilon} \quad (2.27)$$

$$f(\rho_{IV}) = \rho_v + \frac{(\rho_l - \rho_v)^n}{(\rho_l - \rho_v)^{n-1}} \quad n \gg 1 \quad (2.28)$$

where we chose factor [14] $n = 5$.

Other physical criteria have been used the same as at the experimental measurement.

3 EXPERIMENTATION

We performed tests on a smaller cavitation tunnel at the Faculty of Mechanical Engineering at the University of Maribor (FS). The tunnel is designed to research the development of cavitation in various forms of hydraulic hydrofoils. It is a closed type and allows for speeds up to 5 m/s in the tunnel. The cavitation number change is performed by the controlled application of pressure in the system. The flow changed with frequency regulation with driving the electromotor of the pump. Flow rate is measured using an ultrasonic flow-meter.

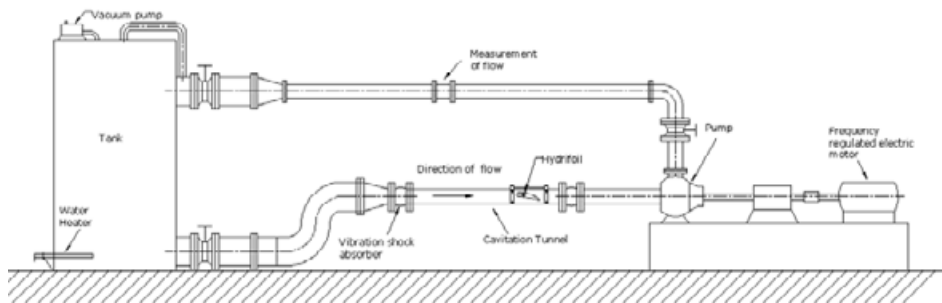


Figure 1: Cavitation tunnel sketch

The contribution was presented to determine the change in lift and drag forces in a hydraulic profile shape. The length of the used profile is $L_0=104$ mm and width is $B=64$ mm, overall length ($l = 17 \times L_0$) of the cavitation plane is part of the tunnel. Material covered the Cu Zn 40, and the variation span of two ball bearings. The hydrofoil was observed through the plexiglass on the two perpendicular sides. The change in lift and drag forces were measured via changes in torsion lever attached to the shaft in a fixed hydrofoil and a dynamometer accuracy of 0.1% (Alborn K - 25). The link shaft and the dynamometer placed with cantilever handle with a length of 94.5 mm. The pressure in the channel was measured before and after the hydrofoil. The cavitation tunnel was insulated from the measuring lines with a rubber shock absorber.

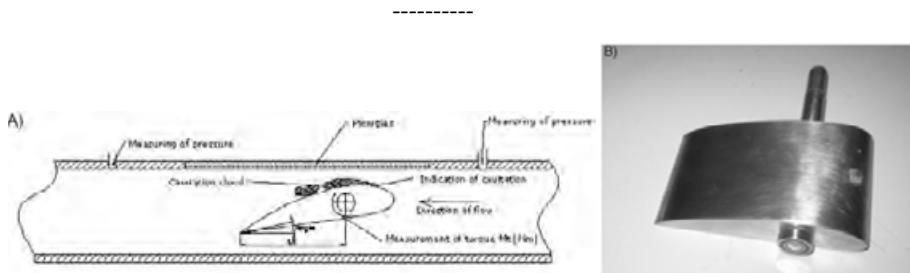


Figure 2: Schematic of the profiled testing hydrofoil

Measurements were performed at different flow velocities in the tunnel (2.7 m/s and 3.3 m/s). The average speed was calculated in the minimum intersection between the hydrofoil and casing plane of the tunnel was between 7.4 m/s and 9.3 m/s. The hydrofoil inclination angle β can be changed on both sides (positive and negative). The zero value $\beta = 0^\circ$ corresponds to the horizontal hydrofoil chord position and positive angles mean lifting of the leading edge (in experiment, an angle 20° of is used). The reference static pressure with a mixture of particles is designated by p_0 (in the case of clean water) is used to determine the cavitation number. Measurement of lift and drag forces was conducted without taking into account the relative friction in the bearings. Visual monitoring of initial cavitation was performed on a metal hydrofoil block located in the middle part of the input hydrofoil surface (nozzle is square: 4 mm x 2 mm x 6 mm). The block was located 12 mm from the inlet edge of the hydrofoil. Measurements were started with pure water (tap water), and continued with three different fractions of particles.

3.1 Preparation of water mixture

For measuring the impact on the development of cavitation, we used particles (sand) material FR 240/F. The density of particle is $\rho_d = 1700 \text{ kg/m}^3$, (diameter of particles is $30 \mu\text{m}$); they are insoluble in water, inert and do not oxidize. Determination of particle size for testing was chosen on the basis of measurements of the actual size of the particles in the Drava River. On the basis of the ascertained real size of river particulates through screens, we obtained the corresponding procedure for the testing of comparable particles in the cavitation tunnel. For measurements in the cavitation tunnel, we used three different fractions of particles. All measurements were performed at the same conditions (flow rates, the reference pressure in the system, temperature).

Table 1: Particle fraction used in the experiment

Mass fraction	$\xi [-]$
Clean water	$\xi = 0$
Fraction 1	$\xi = 0.001$

Fraction 2	$\xi = 0.0016$
Fraction 3	$\xi = 0.0032$

4 ANALYSES OF THE NUMERICAL FLOW AROUND THE HYDROFOIL

The numerical simulation for the flow around the hydrofoil profile using the presented mathematical model was performed with CFX 12.1. The numerical code is based on the finite-volumes method (FVM).

The calculation area is a 3D volume with a size of 900 x 70 x 65 mm, closed from all sides. The area is divided into 5.9×10^5 elements. Geometry hydrofoil and fixing in the cavitation tunnel are presented in detail in the section on the experiment.

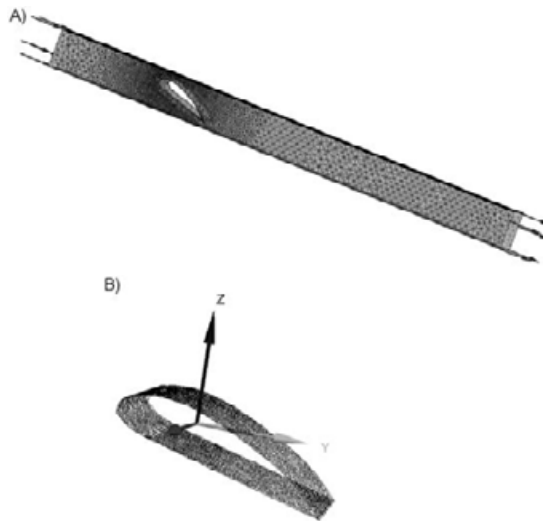


Figure 3: Mesh density near hydrofoil profile surface

The conditions in which the simulations were implemented are as follows: mixture speed is defined at the entry and static pressure at the exit of the domain. Simulations were made by varying the pressure at the exit. Particle fraction was varied at the entrance of the domain; we used a secondary particle diameter of 30 microns. The level of turbulence at the entrance and exit from the computational domain was 5% (viscosity ratio μ_t/μ equal to 10). Interphase drag coefficient C_D for water, particle and vapour are 0.44. We have to use a value for the solids hear viscosity of 0.8 [Pas], dynamic viscosity for particle of 0.01 Pa s and interfacial length scale $l_i = 0.5\text{mm}$ (mixture model). According to experiment and pressure measurements from the

hydrofoil, we needed to account pressure losses to determine the numerical Cavitation number, derived from the measurements.

The cavitation number was achieved interactively, by comparing the the measured and numerical pressure and speed at the hydrofoil. For a converged solution for each step, we assumed a situation in which the amount of the residuals was less then $1 \cdot 10^{-4}$.

5 RESULTS AND DISCUSSION

The experimental study of the impact of particles on change in hydrodynamic forces was carried out with the fractions listed in Table 1. Development of vapour phase in the case of pure water without particles could be observed visually and through the plexiglass. When using a mixture of water with particles, the visual comparisons could not be implemented. Differences were reflected only in the changing of torque. A comparison of simulations carried out and actually developed vapour phase coincides with the entry conditions in the experiment and calculation. Figure 4 shows a visual comparison between experiment and simulation performed on clean water.

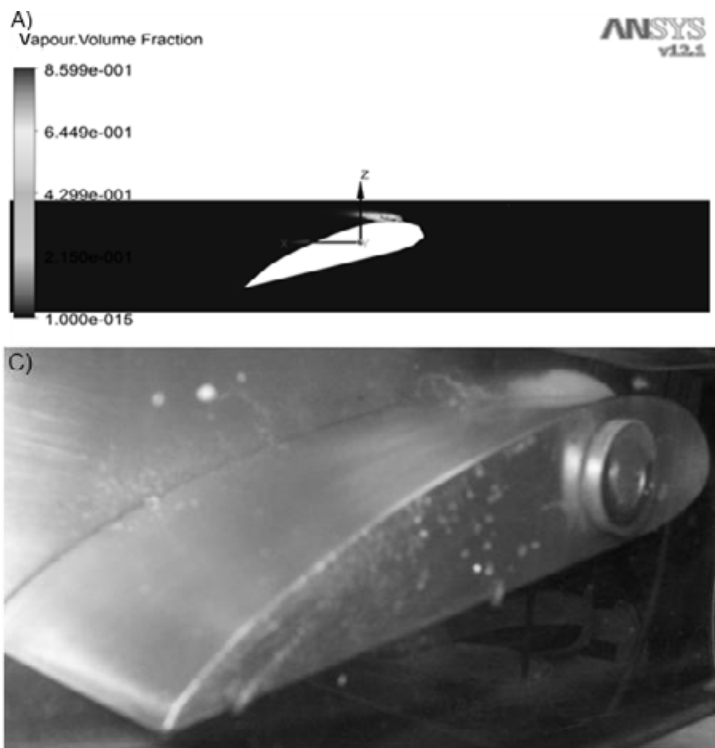




Figure 4: Comparison of simulations of the vapour phase of the experiment

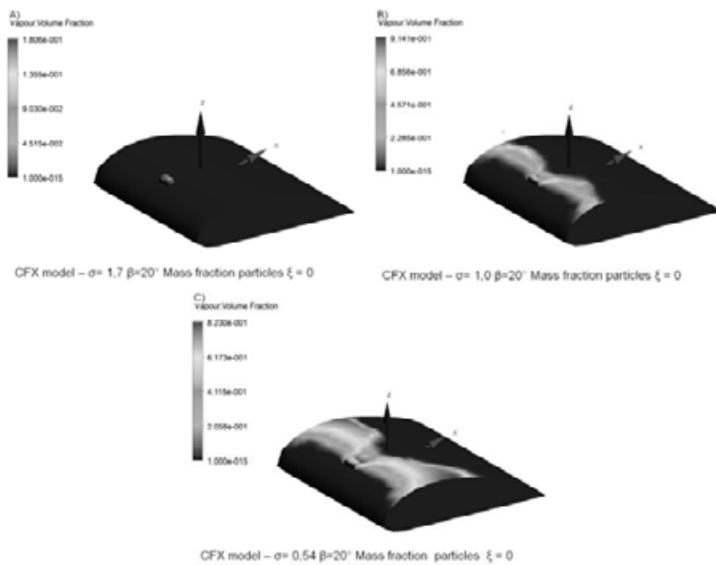


Figure 5: Spots of the vapour phase as a function of cavitation number.

Torque is shown dimensionless as M_t/M_{t0} , where the ratio represents the initial state without cavitation M_{t0} – $\sigma = 1,83$ and M_t , which depends on the reduction of σ . By reducing pressure in the system, we influence the decline in the cavitation number, thus increasing the developed vapour phase.

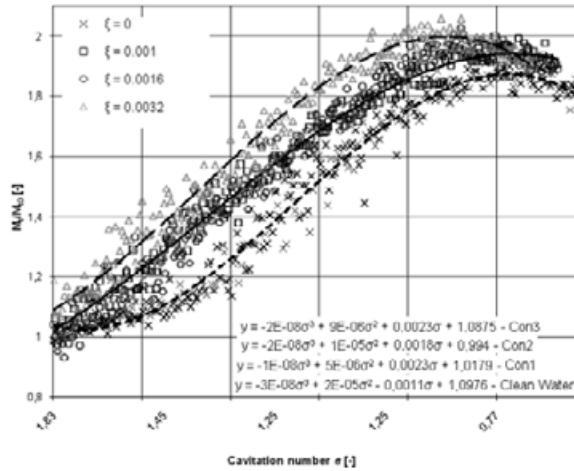


Figure 6: Experimental comparison of torque on hydrofoil using clean water and particle

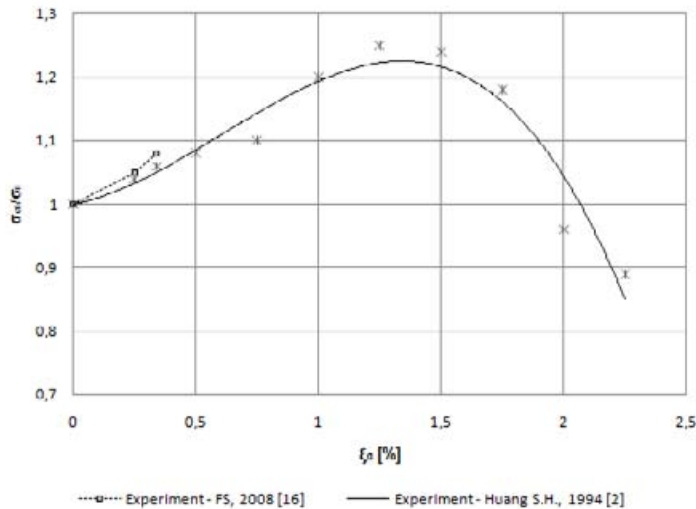


Figure 7: Relation between critical cavitation coefficient and sand concentration

By increasing the gradient hydrofoil angle (Figure 6), the distribution of vapour phases following the suction side of the hydrofoil surface changes. From the measurements, it is clear that regardless of the underlying value of torque, in all cases the torque falls slightly as a result of the formation of the vapour phase on the surface of the hydrofoil. By reducing the reference pressure in the system, the torque does not change linearly, with regard to a change in

pressure, but exponentially. The largest change in momentum can also be seen in the maximum fraction of particles in water, while in comparison with pure water it changes by 8% (cavitation number $\sigma = 0.83$). The experiment shows that by adding sand, the intensity of development of the vapour phase increases at the same cavitation numbers.

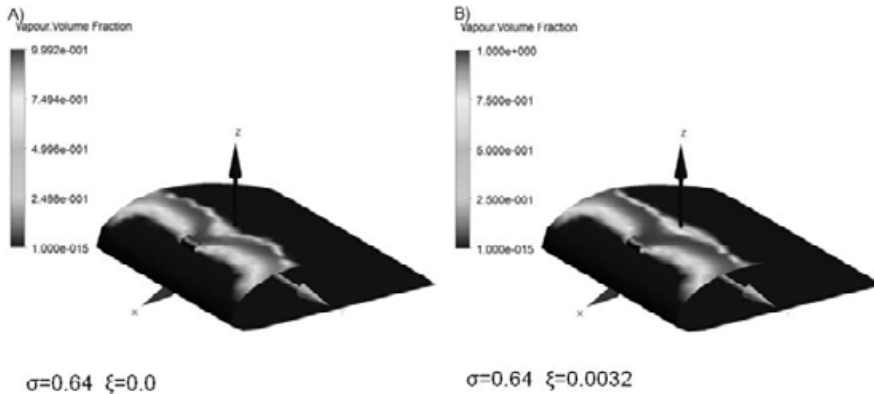


Figure 8: Comparison of vapour volume fraction simulation without particles and with particles at equal cavitation numbers

Figure 8 shows that the particles increase the vapour volume fraction on the hydrofoil profiles NACA. The volume increase depends on the mass fractions of added particles. In the case of added particles, the suction surface is increased surrounded by vapour, as in the case without particles.

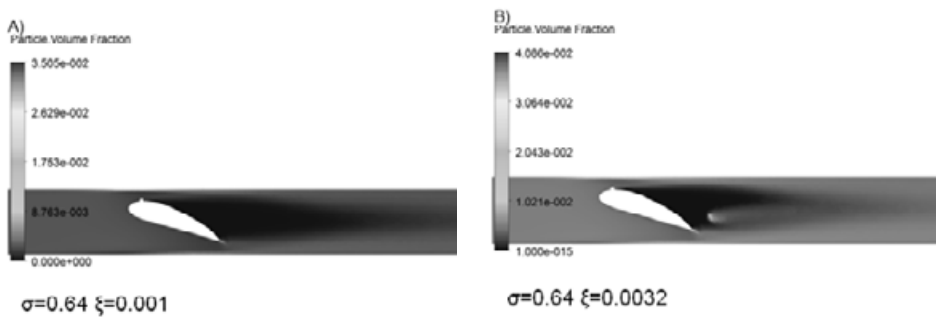


Figure 9: Comparison of simulation with particles at equal cavitation numbers (Particle volume fraction)

Because of increasing turbulence on hydrofoil, the local particle fraction falls. Figures 9A and 9B.

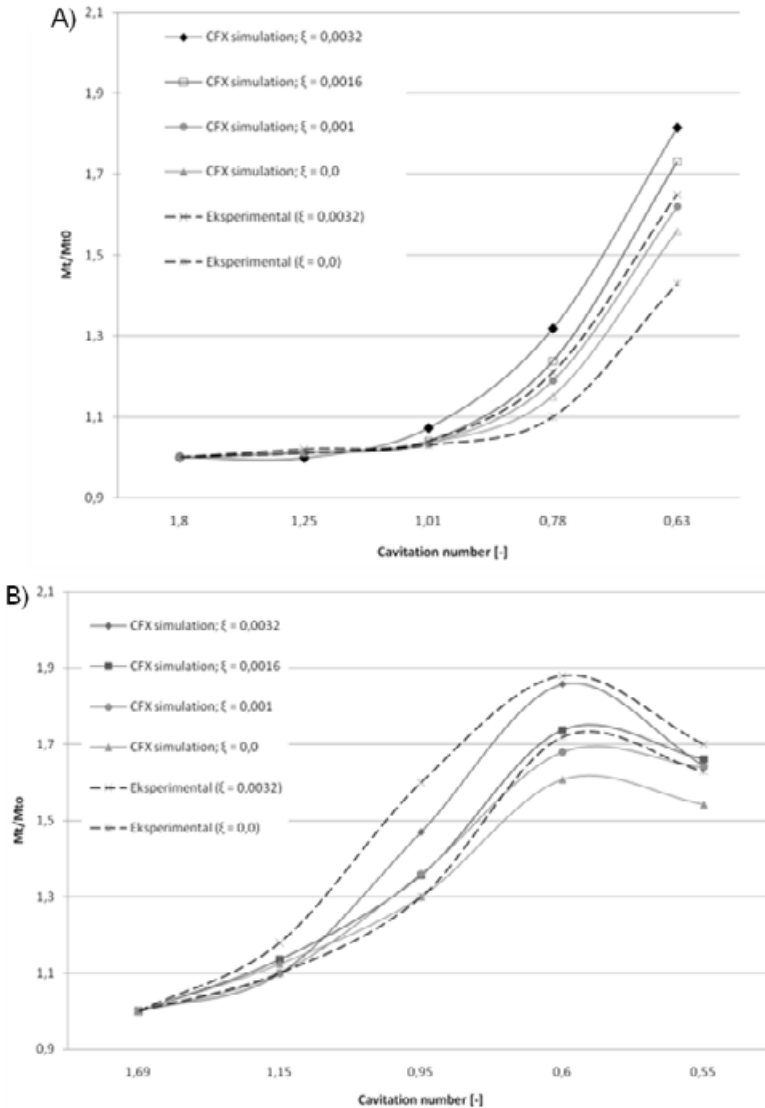


Figure 10: Comparison of torsional moments of simulations and experimental measurements

Figure 10 A shows the particle impact at low-speed ($v_{1,average} = 2.7 \text{ m/s}$) of mixture in a cavitation tunnel. By increasing the proportion of particle fraction, the torque increases. At the cavitation number $\sigma = 0.63$, the cavitation cloud does not yet extend over the entire surface of the suction side hydrofoils. With the increased speed of a mixture of Figure 10 B ($v_{1,average} = 3.3 \text{ m/s}$), the proportion of vapour phase increases, which also significantly affects the increase of torque. The performed simulations show a similar trend in change of torque with clean water and mixture with particles. CFX simulations cover the change of momentum in all three phases (water + particle + vapour).

By reducing the cavitation number, the pressure distribution on the suction side of hydrofoils is increasingly unstable and results in a separation boundary layer, turbulent flow and return flow [3, 10]. Pressure drop increases the intensity of formation of the vapour phase, which results in increasing the area of hydrofoil coverage. With the growing intensity of cavitation, the buoyancy force increases to a maximum value and then begins to fall, as confirmed by experiment and simulation. The growth of buoyancy forces to a certain value has a positive impact on the hydro-mechanical characteristics and increases the efficiency of turbines. The distribution of the pressure after the hydrofoil shows that the pressure developed in the vapour phase is not constant and is not equal to a partial vapour pressure. In reality, the cavitation cloud is composed of a cluster of bubbles, vortices and other structures that are unstable and not constantly in contact with the surface.

6 CONCLUSIONS

In the cavitation tunnel, we explored the effect of particles in the water to change the relative ratio of hydrodynamic forces on a hydrofoil with the NACA profile, using three different fractions of particles in water. When examining the impact of particles on lift and drag forces, we compared the measured (torque) with clean water free of particles. Additional simulations were performed with the same boundary conditions as the experiment was carried out. From the measured values, we have come to the following conclusions:

The location of vapour phase formation and size proportion of surface area covered by the vapour phase is also confirmed by the simulation (Figure 4). The used cavitation model is also appropriate to calculate the hydrodynamic forces on the hydrofoil. The effect of particles in the fluid flow increases torque. The particles impact the increase of faster buoyancy forces, which results in change of torque, as in the case of pure water. The experiment shows that the torque characteristic is relatively the same, but the change is detected earlier than in the case of pure water. This means that the vapour phase occurs at higher cavitation numbers. Particles reduce the turbulence kinetic energy and eddy viscosity of water, which indirectly affects the development of the vapour phase. Particles also affect the reduction of total pressure in the range of vapour phase formation. The pressure drop accelerates the development of the vapour phase. This means that conditions for the vapour phase formation are established sooner. We found that the development of vapor phase shear viscosity significantly affects emissions. Using the parametric analysis, we determined that for the particle diameter < 50 microns and the mass fraction $\xi < 0.005$, we have to use a value for the solids shear viscosity $0.7\text{--}0.8$ Pa s.

References

- [1] **E. Xavier, E. Egusquiza, M. Farthat, F. Avellan, M. Coussirat**, *Detection of cavitation in hydraulic turbines*, Mechanical Systems and Signal Processing 20, (2006), 983–1007
- [2] **C. G. Duan, V. Y. Karelin**, *Abrasive Erosion & Corrosion of Hydraulic Machinery*, International Research Center on Hydraulic Machinery, Beijing; China, Moscow State University of Civil Engineering, (2003), Russia
- [3] **C. Brennen**, *Cavitation and Bubble dynamics*, Oxford University Press, (1995)

-
- [4] **Anys CFX-12.1 Solver Theory**
- [5] **J. Hengyun, Z. Fengzhen, I. Shiyun, H. Chenzhao**, *The Role of Sand Particles on Rapid Destruction of the Cavitation Zone of Hydraulic Turbines*, Institute of Metal Research, Academia Sinica, Shenyang, (1986), China
- [6] **E. Xavier, E. Egusquiza, M. Farthat, F. Avellan**, *Cavitation Erosion Prediction in Hydro Turbines from Onboard Vibrations*, IAHR Symposium on Hydraulic Machinery and Systems, Stockholm, (2004), Sweden
- [7] **F. Bakir, R. Rey, A.G. Gerber, T. Belamri and B. Hutchinson**, *Numerical and Experimental Investigations of the Cavitating Behavior of an Inducer*, *Int J Rotating Machinery*, Vol. 10, (2004), pp. 15–25
- [8] **Z.Y. Mei and Y.L. Wu**, *Review of research on abrasion and cavitation of silt-laden flow through hydraulic turbine runner in China*, Proc. of the 19th IAHR, Section of Hydraulic Machinery and Cavitation, Valencia, (1996), 641–650.
- [9] **M. Farthat, F. Avellan**, *On the Detachment of a Leading Edge Cavitation*, Laboratory For Hydraulic Machines, Swiss Federal Institute of Technology, Lausanne, (2001), (Switzerland)
- [10] **A.P. Keller**, *Cavitation scale effects empirically found relations and the correlation of cavitation number and hydrodynamic coefficients*, Institute of Hydraulic and Water Resources Engineering, Technische Universität München, CAV (2001)
- [11] **B. Širok et al.**, *The Influence of Cavitation Structures on the Erosion of a Symmetrical Hydrofoil in a Cavitation Tunnel*, *Journal of Mechanical Engineering*, (2002)
- [12] **A. K. Singhal, M. M. Athavale**, *Mathematical basis and validation of the full cavitation model*. *Journal of Fluids Engineering*, Vol. 124, (2002), 617-624
- [13] **M. Mikko, T. Veikko**, *On the mixture model for multiphase flow*, Technical Research Centre of Finland, VTT Publications, Espoo (1996), 288. p. 67
- [14] **O. Coutier-Delgosa, R. Fortes-Patella**, *Evaluation of the Turbulence Model Influence on the Numerical Simulations of Unsteady Cavitation*, ASME FEDSM 2003-31188, July14–18, Montreal, Quebec, Canada.
- [15] **T. Aschenbrenner et al.**, *Classification of vortex and cavitation phenomena and assessment of CFD prediction capabilities*, In Proceedings of the 23rd IAHR Symposium on Hydraulic Machinery and Systems, Yokohama, (2006), IAHR
- [16] **B. Gregorc, A. Predin**, *Particle influence on cavitation development at blade profile*, *Journal of Energy Technology*, May 2010, vol. 3. p. 67–82
- [17] **W. H. Brewer and S. A. Kinnas**, *Experimental and computational investigation of sheet cavitation on a hydrofoil*, In FED Cavitation and Multiphase Flow, Proceedings of the ASME/JSME, Fluids Engineering and Laser Anemometry Conference and Exhibition, (1995), 210, 1–15
- [18] **L. Shengcai**, *Cavitation enhancement in silt erosion, Obstacles & way forward*, Fluid Dynamics Research Center, Fifth International Symposium on Cavitation, Osaka, Japan, November, (2003), 1–4
- [19] **L. Shengcai**, *Cavitation enhancement of silt erosion—An envisaged micro model*, *Wear*, Volume 260, Issues 9–10, 31 May (2006), Pages 1145–1150
- [20] **I. Biluš, L. Škrget, A. Predin, M. Hriberšek**, *Experimental and numerical analyses of the cavitation flows around hydrofoil*, *Journal of Mechanical Engineering*, (2005), 103–118

- [21] **A. K. Singhal, N. Vaidya, A. D. Leonard**, *Multi- dimensional Simulation of Cavitating Flows Using a PDF Model for Phase Change*, Proceeding of ASME Fluids Engineering Division Summer Meeting, Vancouver, ASME, (1997), 4:1–8.

Nomenclature

k	turbulent kinetic energy production [m^2s^{-2}]
p	thermodynamic pressure [Pa]
p_t	total pressure [Pa]
v	characteristic velocity [m/s]
ε	disipation velocity of turbulent kinetic energy [m^2s^{-3}]
μ	viscosity [Pa s]
μ_t	turbulent viscosity [Pa s]
ρ	density [kg/m^3]
R	bubble radius [m]
r_{nuc}	nuclei radius [m]
ξ_c	mass concentration [kg/m^3]
ξ	mass fraction [-]
α	volume fraction [-]
$\sigma = (p - p_v) / (\frac{\rho v_{ref}^2}{2})$	cavitation number [-]
F_{con}	coefficient [-]
F_{vap}	coefficient [-]
C_D	drag coefficient [-]

Subscripts

l	liquid phase
d	dispersed phase
v	vapour phase
p	particle
m	mixture

FAILURE ANALYSIS OF A RAILWAY BRAKE DISC

ANALIZA POŠKODB ŽELEZNIŠKEGA ZAVORNEGA DISKA

Blaž Šamec[✉], Grega Oder, Tone Lerher, Iztok Potrč

Keywords: railway brake disc, thermo-mechanical analysis, numerical analysis, redesign

Abstract

A certain number of railway brake discs, made of gray cast iron, show the presence of small cracks after only a few thousand kilometres. To investigate the main causes of a brake disc failure, a numerical analysis was done, using ABAQUS software. The analysis resulted from a physical model of heat flux in dependence of braking time. The physical model was applied considering all demands and presumptions given by industry representatives.

Povzetek

Na določenem številu železniških zavornih diskov, narejenih iz sive litine, so nastale majhne razpoke že po nekaj tisoč kilometrih. Da bi raziskali glavne vzroke za odpoved zavornih diskov, je bila opravljena numerična analiza z uporabo programske opreme ABAQUS. Termična analiza diska je izhajala iz fizikalnega modela za določitev toplotnega toka v odvisnosti od časa zaviranja. Pri uporabi fizikalnega modela, so bile upoštevane vse zahteve in predpostavke podane s strani naročnika projekta.

[✉] Corresponding author: Blaž Šamec, Tel.: +386 2 2207721, Mailing address: University of Maribor, Faculty of Mechanical Engineering, Smetanova 17, 2000 Maribor, Slovenia, E-mail address: blaz.samec@uni-mb.si

1 INTRODUCTION

Disc brakes, not only for railway applications but in all vehicle applications, are considered to be safety components. Therefore, their reliability during service is essential.

Brakes are essentially a mechanism to change energy types. When a vehicle is moving with speed, it has kinetic energy. Applying the brakes, the pads that press against the brake rotor convert this energy into thermal energy. The cooling of the brakes dissipates the heat and the vehicle slows down [1].

With friction brakes, the thermal phenomenon is of great importance. Vehicle deceleration and stopping rely entirely on friction (sliding contact), and the process must be predictable and reliable in order to enable safe operation. It should be noted that in addition to substantial mechanical forces, friction heat generation is extremely high. In heavy duty brake application, the heat flux at the interface is of the order of MW/m^2 . The heat generated during braking causes the temperature to increase at the interface, which spreads quickly through the brake components. Such severe thermal processes modify the friction properties of the materials in contact, cause wear and, more generally, result in component deflection. All these changes inevitably affect brake performance and life [2].

A certain number of railway disc brakes, made of gray cast iron, show the presence of small cracks only after a few thousand kilometres. To investigate the main causes of brake disc failure, a numerical analysis was done, using ABAQUS software. The numerical analysis resulted from a physical model of heat flux dependent on braking time [3]. A physical model was employed, considering all demands and presumptions given by industry representatives.

A brake disc consists of two parts, which are mounted directly onto the wheel from each side (Fig. 1). Each part is attached to the wheel with 3 hexagon socket bolts $\text{M20} \times 50$ (fastening moment of bolts is 580 Nm) and with 3 pins 20×70 (DIN 7979). The diameter of a brake disc is 780 mm and the weight is 84.3 kg (one part of a brake disc). Brake discs are made of gray cast iron (EN-GJL-250). The reason this material is used is because of its low cost, ease of manufacturing, strength and resistance to thermal loading.

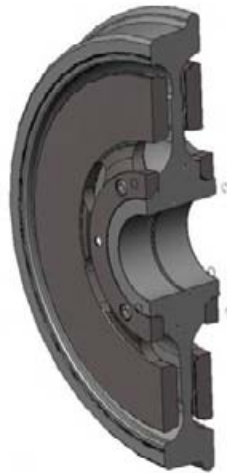


Figure 1: Cross-section of a railway wheel with a brake disc

2 THERMO-MECHANICAL ANALYSIS

During deceleration, the load shifts to the front wheels so that a large fraction of the work-of-braking is done by the front brakes. Brake discs on a front bogie are more loaded than the rear ones. In the calculation, a 60/40 load distribution between front and rear bogie was taken into consideration. Because of greater loads, the front bogie's brake discs were analyzed. Taking into account the 60/40 load distribution and four wheels per bogie, 15% of braking force is carried by one disc.

The activity of braking pads on a rotating disc generates heat flux on a disc surface. The relation between full braking power and no braking is used for a calculation of the thermal loading of disc brakes. Force, acting on a brake disc, is calculated from data in Table 1.

Table 1: Vehicle data

Vehicle mass	67500 kg
Initial speed	39 m/s
Deceleration	1.3 m/s ²
Stop time	30 s
Effective brake disc radius	0.325 m
Wheel radius	0.475 m

It is assumed that deceleration is constant, that the major part of the energy is kinetic and that the mechanical energy is completely converted into heat. The power dissipated by each brake

disc is equal to the instantaneous heat flux into the rotor face. Brake clamp load is modelled as a combination of pressure and friction on the surface of 400 cm^2 on a section of a brake disc.

Table 2: Loads on a brake disc

Initial temperature	350 °C
Heat flux	(changing with time)
Centrifugal forces	(changing with time)
Pre-stressed bolts (pressure on the bolt seat)	285 MPa
Brake clamp pressure	0.56 MPa
Surface traction of brake pads	0.24 MPa

3 RESULTS AND CONSIDERATIONS

As heat flux is at maximum at the beginning of the brake cycle, the temperature rises rapidly; however, at the end of the brake cycle the heat flux tends to zero and the temperature decreases, owing to heat diffusion into the disc. Figure 2 shows the temperature on the frictional surface of a disc brake.

The maximum stresses, in the value of 1095 MPa, occur 20 seconds after the start of braking. Von Mises stresses are explicit around holes for the mounting bolts (Figure 3). It is estimated that the actual peak stress is lower. In to our opinion, stress of 1095 MPa is a model "error" due to the geometric singularity and regarding to the thermo-elastic material model (the linear elastic material model was used, no plastification of material was considered). However, the maximum stress is a result of a change in boundary conditions, because the bolt hole is not fully supported (Figure 4).

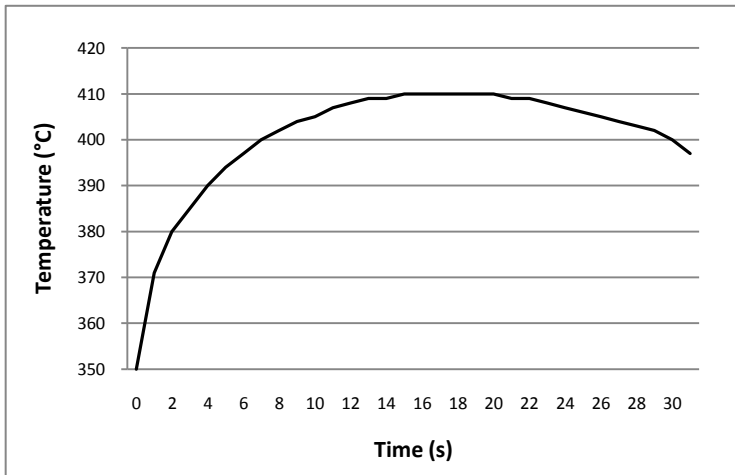


Figure 2: Temperature on the frictional surface

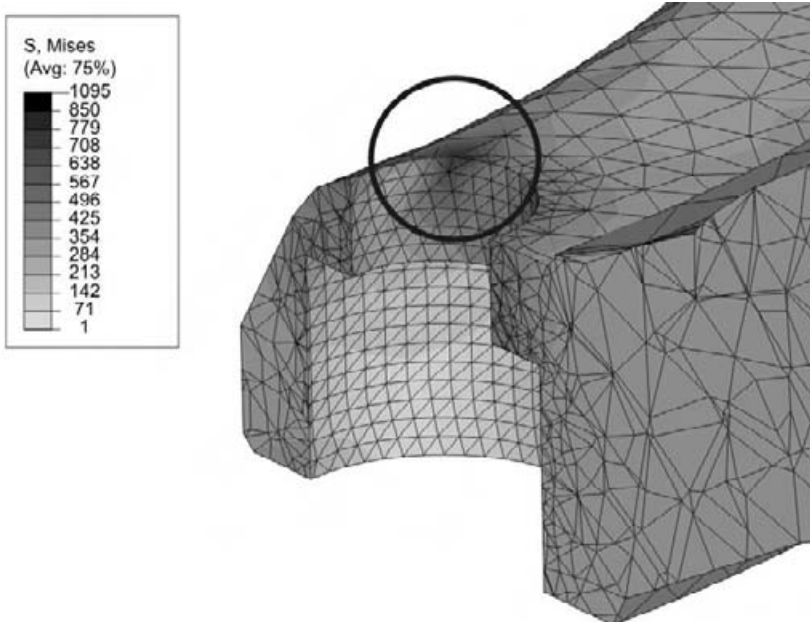


Figure 3: Concentration of stresses around hole for mounting bolts

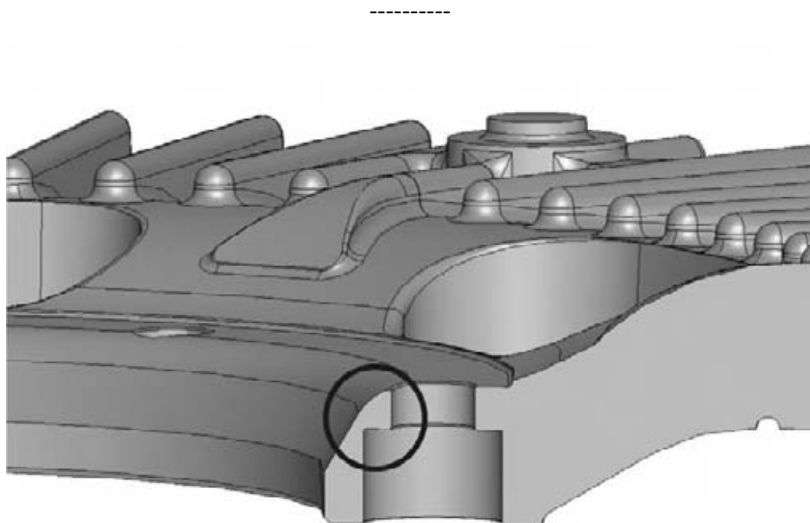


Figure 4: Initial hole design

4 REDESIGN OF A BRAKE DISC

A redesign of a brake disc was suggested, so that holes for the mounting bolts have lower depths and are fully supported (Figure 5). Changing the brake disc material to nodular (spheroidal) graphite cast iron (EN-GJS-400-18) has also been proposed. The selection of this material is based on its superior toughness, needed to endure the thermal elastic-plastic stresses around the yield strength. The microstructure of the material remains stable up to about 500 °C [4].

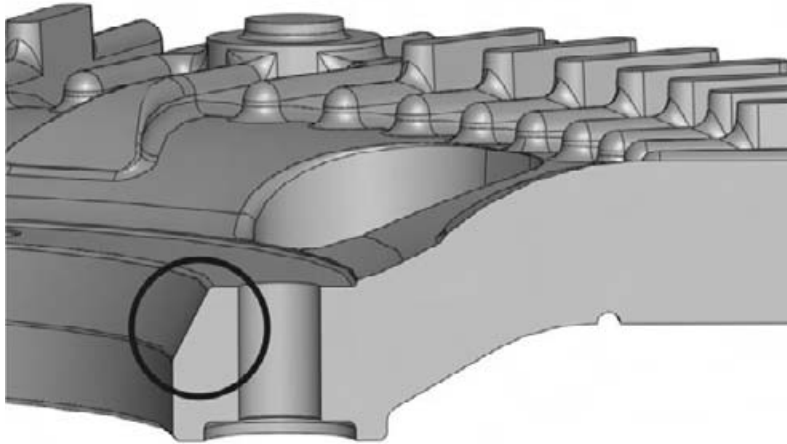


Figure 5: Redesign of a hole

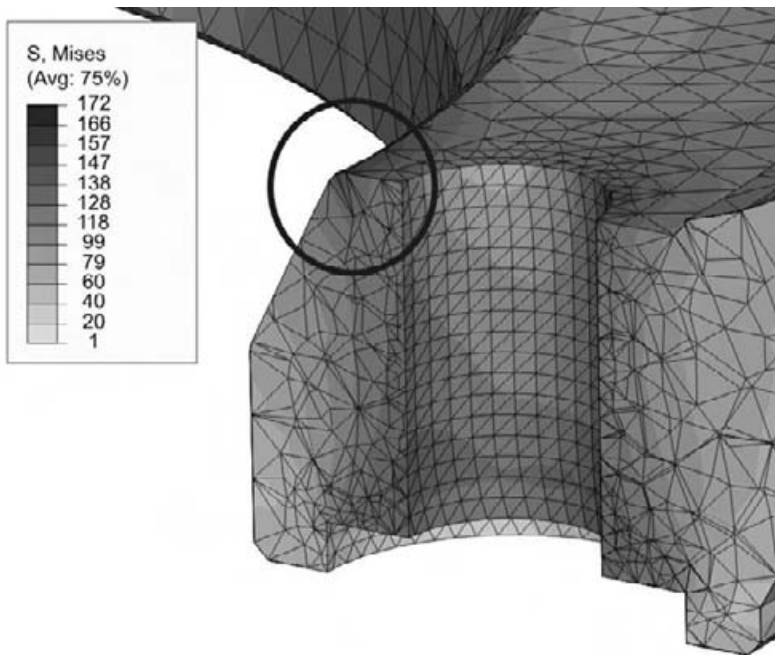


Figure 6: Concentration of stresses around hole after the redesign of a brake disc

Bolts are fasten with a moment of 580 Nm, which is, considering DIN 267, the maximum permissible moment of fastening for selected bolts (property class of bolts is 10.9, which equals 900 MPa of tensile stress). Braking torque, which can be transferred via wheel/disk, based on a force of pre-stressed bolts, is approximately 4.6 times greater than required for the most unfavourable model of braking. Given the minimal pre-stressed force of bolts and taking into

consideration the necessary safety factor ($\nu = 2.5$), the minimum required moment of fastening bolts is 315 Nm. This has reduced the pressure on the bolt seat from the previous 285 MPa to 155 MPa.

Numerical analysis of a redesigned brake disc shows a distinctive reduction of stresses around holes for mounting bolts. In this case, von Mises stress decreased from about 1100 MPa to 170 MPa (Figure 6).

5 CONCLUSIONS

The analysis herein shows that brake disc failure is a consequence of an unfavourable design and excessive fastening moment of bolts, which was the main reason for crack initiation. After redesign of a brake disc and recalculation of fastening moment for bolts, distinctive reduction of von Mises stress can be seen around holes. Stresses decreased to 170 MPa, i.e. to only 15% of their initial value.

References

- [1] **F. Talati, S. Jalalifar.** *Analysis of heat conduction in a disk brake system.* Heat and Mass Transfer (2009), vol. 45, no. 8, pp. 1047–1059.
- [2] **D. Majcherczak, P. Dufrenoy, Y. Berthier.** *Tribological, thermal and mechanical coupling aspects of the dry sliding contact.* Tribology International (2007), vol. 40, no. 5, pp. 834–843.
- [3] **T.J. Mackin, S.C. Noe, K.J. Ball, B.C. Bedell, D.P. Bim-Merle, M.C. Bingaman, D.M. Bomleny, G.J. Chemlir, D.B. Clayton, H.A. Evans, R. Gau, J.L. Hart, J.S. Karney, B.P. Kiple, R.C. Kaluga, P. Kung, A.K. Law, D. Lim, R.C. Merema, B.M. Miller, T.R. Miller, T.J. Nielson, T.M. O'Shea, M.T. Olson, H.A. Padilla, B.W. Penner, C. Penny, R.P. Peterson, V.C. Polidoro, A. Raghu, B.R. Resor, B.J. Robinson, D. Schambach, B.D. Snyder, E. Tom, R.R. Tschantz, B.M. Walker, K.E. Wasielewski, T.R. Webb, S.A. Wise, R.S. Yang, R.S. Zimmerman.** *Thermal cracking in disc brakes.* Engineering Failure Analysis (2002), vol. 9, no. 1, pp. 63–76.
- [4] **C.M. Sonsino, H. Hanselka.** *Fatigue life assessment of cast nodular iron disc brakes for railway vehicles.* Revue de Metallurgie. Cahiers D'Informations Techniques (2007), vol. 104, no. 11, pp. 562–568.



AUTHOR INSTRUCTIONS (MAIN TITLE)

SLOVENIAN TITLE

Authors, Corresponding author^{3†}

Key words: (Up to 10 keywords)

Abstract

Abstract should be up to 500 words long, with no pictures, photos, equations, tables, only text.

Povzetek

(In Slovenian language)

Submission of Manuscripts: All manuscripts must be submitted in English by e-mail to the editorial office at jet@uni-mb.si to ensure fast processing. Instructions for authors are also available online at <http://www.fe.uni-mb.si/si/jet.html> .

Preparation of manuscripts: Manuscripts must be typed in English in prescribed journal form (Word editor). A Word template is available at the Journal Home page.

A title page consists of the main title in the English and Slovenian languages; the author(s) name(s) as well as the address, affiliation, E-mail address, telephone and fax numbers of author(s). Corresponding author must be indicated.

Main title: should be centred and written with capital letters (ARIAL **bold** 18 pt), in first paragraph in English language, in second paragraph in Slovenian language.

Key words: A list of 3 up to 6 key words is essential for indexing purposes. (CALIBRI 10pt)

Abstract: Abstract should be up to 500 words long, with no pictures, photos, equations, tables, - text only.

Povzetek: - Abstract in Slovenian language.

^{3†} Corresponding author and other authors: Title, Name and Surname, Tel.: +XXX x xxx xxx, Fax: +XXX x xxx xxx, Mailing address: xxxxxxxxxxxxxxxxxxxxxxxxxxxxxxxxxxxx, E-mail address: email@xxx.xx

Main text should be structured logically in chapters, sections and sub-sections. Type of letters is Calibri, 10pt, full justified.

Units and abbreviations: Required are SI units. Abbreviations must be given in text when first mentioned.

Proofreading: The proof will be send by e-mail to the corresponding author, who is required to make their proof corrections. The corresponding author is responsible to introduce corrections of data in the paper. The Editors are not responsible for damage or loss of manuscripts submitted. Contributors are advised to keep copies of their manuscript, illustrations and all other materials.

The statements, opinions and data contained in this publication are solely those of the individual authors and not of the publisher and the Editors. Neither the publisher nor the Editors can accept any legal responsibility for errors that could appear during the process.

Copyright: Submissions of a publication article implies transfer of the copyright from the author(s) to the publisher upon acceptance of the paper. Accepted papers become the permanent property of “Journal of Energy Technology”. All articles published in this journal are protected by copyright, which covers the exclusive rights to reproduce and distribute the article as well as all translation rights. No material can be published without written permission of the publisher.

Chapter examples:

1 MAIN CHAPTER

(Arial bold, 12pt, after paragraph 6pt space)

1.1 Section

(Arial bold, 11pt, after paragraph 6pt space)

1.1.1 Sub-section

(Arial bold, 10pt, after paragraph 6pt space)

Example of Equation (lined 2 cm from left margin, equation number in normal brackets (section.equation number), lined right margin, paragraph space 6pt before in after line):

$$c = \sqrt{a^2 + b^2} \tag{1.1}$$

Tables should have a legend that includes the title of the table at the top of the table. Each table should be cited in the text.

Table legend example:

Table 1: Name of the table (centred, on top of the table)

Figures and images should be labelled sequentially numbered (Arabic numbers) and cited in the text – Fig.1 or Figure 1. The legend should be below the image, picture, photo or drawing.

Figure legend example:

Figure 1: Name of the figure (centred, on bottom of image, photo, or drawing)

References

[1] **Name. Surname:** *Title*, Publisher, p.p., Year of Publication

Example of reference-1 citation: In text, Predin, [1], text continue. **(Reference number order!)**

SiPRO
INŽENIRING

Gen
ENERGIJA


FEKU
Nepremičnine
Tel: 02 235 23 20, gsm: 041 859 442,
www.feku.si, info@feku.si

JET

JET
Journal of ENERGY TECHNOLOGY

Vol. 3/4 2010

UNIVERSITY OF MARIBOR, FACULTY OF ENERGY TECHNOLOGY



9 771855 574008

ISSN 1855-5748